Analysis and Design of Watermarking Algorithms for Improved Resistance to Compression

Chuhong Fei, Deepa Kundur, *Senior Member, IEEE*, and Raymond H. Kwong, *Member, IEEE*

***Abstract*—We study the performance of robust digital watermarking approaches in the presence of lossy compression by introducing practical analysis methodologies. Correlation expressions between the embedded watermark and the extracted watermark are derived to determine the optimal watermarking domain to maximize data hiding rates for spread spectrum and quantization watermarking. It is determined both theoretically and through simulations that the embedding strategy, in addition to the transform used for lossy compression, dictate the optimal transform for watermarking. Through analytic comparisons, we develop a novel hybrid watermarking algorithm that exploits the best of both approaches for greater resilience to JPEG compression.**

***Index Terms*—Data hiding, digital watermarking, hybrid watermarking, JPEG compression, perceptual coding, quantization.**

I. Introduction

DIGITAL watermarking technology is emerging as a solution to a broad class of information communication challenges such as self-healing data, broadcast monitoring, and signal tagging. In these applications, compression is the most common form of incidental distortion to limit the robustness of watermarking. This paper deals with the performance analysis and design of watermark embedding strategies robust to perceptual coding. *Perceptual coding* is the lossy compression of multimedia using human perceptual models. Both compression and watermarking are based on the premise that minor modifications of the signal representation will not be noticeable in the displayed content. For compression, these modifications are imposed to reduce the number of bits required for storage. For watermarking, the changes are used in detecting the watermark. To successfully integrate perceptual coding with watermarking, we must identify an appropriate compromise so that both processes can simultaneously achieve their tasks.

In previous work, Wolfgang *et al.* [1] investigate the performance of discrete cosine transform (DCT)- and discrete wavelet transform (DWT)-based spread spectrum watermarking techniques for color image compression algorithms using the DCT and the DWT. They assert that matching the watermark and coding transforms improves performance. However, their simulation results are somewhat inconclusive and there is no theoretical motivation for their hypothesis. Kundur and Hatzinakos [2] argue both analytically and through the use of simulation results that the use of the same transform for both watermarking and compression results in suboptimal performance for repetition-code-based quantization watermarking. Ramkumar and Akansu [3], [4] use information theory to compare the capacities of spread spectrum data hiding in the presence of compression for different block transforms. They conclude that transforms which have poor energy compaction and are not suitable for compression, like the Hadamard and Hartley transforms, are preferable choices for higher capacity requirements. These inconsistencies in the literature raise the following questions that we address in this work. What is the best embedding transform for robustness against lossy compression? For such a scenario, is spread spectrum or quantization-based embedding superior?

We answer these questions through the following contributions.

- We introduce a methodology to analytically determine the relative performance of a watermark embedding domain in the presence of block-based lossy compression. Spread spectrum [5]–[9] and quantization-based [10]–[12] embedding approaches are both considered.
- By characterizing the strengths of these approaches, we design a novel hybrid watermarking algorithm that exploits the best of both digital watermarking techniques.
- We verify our theoretical observations through software implementation, testing, and comparisons of the spread spectrum, quantization-based, and hybrid watermarking schemes.

This work can also be considered an extension of some existing research [10], [13]–[17]. In [13], [14], Eggers and Girod provide a detailed analysis of quantization effects on spread spectrum watermarking schemes in the DCT domain. In this paper, we build upon these results for application to general watermarking transforms. In particular, our work on spread spectrum watermarking analysis can be regarded as an expansion of their work where we use a parallel array of 64 quantizers with coupled signal inputs.

Similarly, our work on developing a hybrid method of watermarking can be viewed as a formalization of the ideas first presented by Wu and Yu [10], [15] on combining two different watermark embedding strategies for embedding information in the 8×8 block DCT coefficients of host video. Quantization watermarking [10] is used for embedding in the "low frequencies," and spread spectrum watermerking in the "high frequencies." Part of the work in this paper is considered

Manuscript received May 6, 2002; revised July 10, 2003. The associate editor coordinating the review of this manuscript and approving it for publication was Prof. Bruno Carpentieri.

C. Fei and R. H. Kwong are with the Edward S. Rogers Sr. Department of Electrical and Computer Engineering, University of Toronto, Toronto, ON M5S 3G4 Canada (e-mail: fei@control.toronto.edu; kwong@control.toronto.edu).

D. Kundur is with the Department of Electrical Engineering, Texas A&M University, College Station, TX 77843-3128 USA (e-mail: deepa@ee.tamu.edu).

Digital Object Identifier 10.1109/TIP.2004.823830

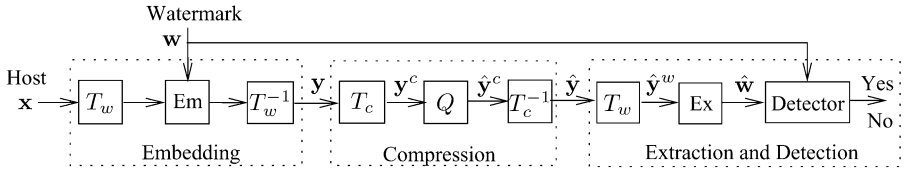

Fig. 1. Proposed joint watermarking and compression scenario. Watermark embedding and compression occur in the T_w and T_c domains, respectively.

an extension of [15] for which we analytically derive a way to partition the coefficients for different embedding strategies to maximize robustness.

Overall, the ideas presented in this paper is also an extension of previous work by the authors in [16], [17]. A more accurate model to incorporate quantization from compression for spread spectrum watermarking is employed. A covariance model for the host image is no longer assumed and a generalized Gaussian structure for the host image coefficients is used. Furthermore, we extend our quantization-based watermarking analysis to encompass more robust schemes recently developed by [18], [19].

The next section formulates the specific problem we consider highlighting the models and approaches we employ. Section III introduces spread spectrum watermarking and analyzes its behavior to JPEG compression. Section IV similarly focuses on quantization-based watermarking. We present our hybrid watermarking algorithm in Section V, followed by final remarks in Section VI.

II. Problem Formulation

A. Watermarking in the Presence of Compression

A block diagram of watermarking in the presence of lossy compression is shown in Fig. 1. The embedding process occurs in a *watermark domain* through application of an orthonormal transformation T_w on the original host image $\mathbf{x}$ to produce coefficients in which to embed the watermark. Taking the inverse transform T_w^{-1} of the marked coefficients produces the watermarked image $\mathbf{y}$ that is perceptually identical to $\mathbf{x}$. Lossy compression, possibly applied by a third party, occurs after embedding in our applications of interest, and is modeled as quantization Q of signal coefficients in a specified *compression domain*; the associated orthogonal compression transform is denoted T_c and the compressed watermarked image by $\hat{\mathbf{y}}$. At the receiver, the hidden message $\hat{\mathbf{w}}$ is extracted from the "corrupted" watermarked image $\hat{\mathbf{y}}^w$ in the watermark domain. Our study focuses on *blind* watermarking where the original host image $\mathbf{x}$ is not available at the watermark receiver. Our scenario models applications in which compression is applied after and separate from watermark embedding which may often occur in broadcast applications among others.

Given the scenario of Fig. 1, our goal, in part, is to determine a good T_w for a given T_c for spread spectrum and quantization watermarking. The most commonly used transforms in image processing include the DCT, DWT, Hadamard transform, discrete Fourier transform (DFT), Karhunen Loeve transform (KLT), and slant transform. The results in this paper rank these popular transformations for their effectiveness in practical robust watermarking in the presence of compression. We can fix T_c to be the 8×8 block DCT transform, to apply our results to JPEG compression. It should be emphasized that we are not interested in solving an optimization problem to determine the best T_w for a given T_c. Instead, we believe it is more useful to rank commonly used transforms as a function of compression level to give guidance on how to choose an appropriate watermarking approach from the existing body of literature.

B. Watermark Embedding and Detection

For compatibility with compression, we assume a block-based structure for watermarking. That is, if nonoverlapping 8×8 blocks are transformed using T_c and quantized for block-based compression, then these same 8×8 blocks are independently processed for watermarking in a possibly different domain T_w. Thus, our coding and watermark blocks are *synchronized*. By imposing this restriction, we can directly related our results to the effects of varying the watermark and compression domains. The issue of desynchronization of the blocks on the watermark detection is investigated through simulations in Section V-D.

Therefore, for watermark processing, the host watermark images are naturally partitioned into 8×8 blocks which are numbered in column scan order using an argument block index k. The image coefficients within a given 8×8 block are represented with a subscript i (or j) also numbered in column scan order. A superscript of w or c is used to denote the signal coefficients in the watermark or compression domains, respectively. For example, $x_i^w(k)$ is the ith host image coefficient in the kth block of the watermark domain, and $y_j^c(k)$ is the jth watermarked image coefficient of the kth block of the compression domain.

In this work, we take, in part, a data communications perspective to the watermarking problem in which watermark embedding is analogous to channel coding and modulation, detection to a communication receiver and the effective communication channel that we call the *watermark channel* is characterized by the host image and compression process. Within this framework, we introduce the notion of *subchannels*. Specifically, in the watermark domain, the ith coefficient of an 8×8 image block is considered to belong to the ith subchannel of the overall watermark channel for $i = 1, 2, \ldots, N$ where $N = 8^2 = 64$. If there are a total of K 8×8 blocks in an image for watermarking, then each block "carries" one symbol for each subchannel i. In an entire image with K 8×8 blocks we can embed an K-*length* symbol-block for each subchannel. For an image such as Lena of size 512×512, there are a total of $K = 4096$ blocks. Thus, we can embed a watermark sequence of length 4096 for each subchannel.

The presence of a watermark in the received image $\hat{\mathbf{y}}$ is detected by a correlation detector. A practically useful detection measure used for spread spectrum watermarking is the correlation coefficient [20]. Let $w_i(1), w_i(2), \cdots, w_i(K)$ be the water-

mark and $\hat{w}_i(1), \hat{w}_i(2), \cdots, \hat{w}_i(K)$ be the extracted watermark in subchannel i. The correlation coefficient for each subchannel i is given by

$$\rho_i = \frac{\frac{1}{K}\sum_{k=1}^{K} w_i(k)\hat{w}_i(k)}{\sqrt{\sigma_{w_i}^2}\sqrt{\frac{1}{K}\sum_{k=1}^{K}\hat{w}_i^2(k)}} \tag{1}$$

where $\sigma_{w_i}^2$ is the variance (i.e., energy) of the watermark and $(1/K)\sum_{k=1}^{K}\hat{w}_i^2(k)$ is the sample variance of the extracted watermark in subchannel i.

To detect the presence of watermark in an image containing 64 subchannels, the average correlation coefficient over all subchannels is computed

$$\tilde{\rho} = \frac{1}{64}\sum_{i=1}^{64}\rho_i. \tag{2}$$

Then the presence of watermark is detected by comparing the average correlation coefficient with a pre-defined threshold $\mathcal{T}$. The watermark is considered to be present if the average correlation coefficient is greater than the threshold $\mathcal{T}$.

C. Figures of Merit

We use the following figures of merit to measure the appropriateness of the different transforms for robust watermarking. The first measure is the expected average correlation coefficient $E\{\tilde{\rho}\}$. We assume the watermark sequence $w_i(k)$, $k = 1, 2, \cdots$ and the extracted watermark sequence $\hat{w}_i(k)$, $k = 1, 2, \cdots$ are zero mean independent and identically distributed sources drawn from random variables w_i and $\hat{w}_i$, respectively. We also assume the extracted watermark sequence is ergodic. For sufficiently large block number K, the sample variance of the extracted watermark $(1/K)\sum_{k=1}^{K}\hat{w}_i^2(k)$ in (1) approaches the variance of $\hat{w}_i$ by the law of large numbers. Thus, the expected average correlation coefficient is approximated as follows:

$$E\{\tilde{\rho}\} = \frac{1}{64}\sum_{i=1}^{64}E\{\rho_i\} \tag{3}$$

$$E\{\rho_i\} = \frac{E\{w_i\hat{w}_i\}}{\sqrt{E\{w_i^2\}E\{\hat{w}_i^2\}}}. \tag{4}$$

In an ideal case in which the lengths of the watermarks and host image coefficients go to infinite, the correlation coefficient approaches its expectation by the law of large numbers. Hence, the expectation value of the average correlation coefficient measures the performance of the spread spectrum watermarking scheme with infinite length watermarks.

The second practical measure, for finite length watermarks, is the watermark detection error probability defined as the probability that the correlation detector fails to detect a watermark that is indeed present, that is

$$p_e = P\{\tilde{\rho} < \mathcal{T} | \text{the watermark is present}\}. \tag{5}$$

For sufficiently large block number K, by the central limit theorem, each correlation coefficient ρ_i in subchannel i is modeled by a Gaussian random variable with expectation given in (4) and variance approximated by

$$Var\{\rho_i\} = \frac{Var\{w_i\hat{w}_i\}}{K\sqrt{E\{w_i^2\}E\{\hat{w}_i^2\}}}. \tag{6}$$

Then the average correlation coefficient $\tilde{\rho}$ is modeled by a Gaussian variable with expectation given in (3) and variance as follows:

$$Var\{\tilde{\rho}\} = \frac{1}{64^2}\sum_{i=1}^{64}Var\{\rho_i\}. \tag{7}$$

A watermark detection error occurs when the measured average correlation coefficient is less than a pre-defined threshold $\mathcal{T}$. Thus, the watermark detection error probability is estimated by

$$p_e = \text{erf}\left(\frac{\mathcal{T} - E\{\tilde{\rho}\}}{\sqrt{Var\{\tilde{\rho}\}}}\right) \tag{8}$$

where the error function $\text{erf}(x) = (1/\sqrt{2\pi})\int_{-\infty}^{x} e^{-t^2/2}dt$.

There are primarily two types of error probability associated with a watermarking system [20]. One is the false negative error probability, which is the probability that the detector fails to detect the presence of a watermark, as given in (5). The other dual is the false positive probability, which is the probability of detecting the watermark when it is not there. When a watermark is not embedded in an image, the extracted watermark from the image is independent of the watermark, thus the correlation coefficient between the watermark and the extracted watermark is zero mean with variance approximated by $1/K$ [20]. Thus, the choice of watermark transform domain does not affect the false positive probability and we, therefore, only focus on the false negative error probability defined in (5) in our paper.

III. Spread-Spectrum Watermarking

In this section, we discuss our model for spread spectrum watermarking. Spread spectrum watermarking schemes borrow ideas from spread spectrum communications. In spread spectrum communications, a narrowband signal is transmitted over a much larger bandwidth such that the signal energy present in any single frequency is imperceptible. Similarly, in spread spectrum watermarking schemes, a watermark is spread over many samples of the host signal by adding a low energy pseudo-randomly generated white noise sequence. This specific pseudonoise sequence is detected by correlating the original watermark sequence with the watermarked signal itself for blind watermarking where the host image is not available for extraction.

Let $\mathbf{x}^w = [x_1^w, x_2^w, \cdots, x_N^w]^T$ (where $[\cdot]^T$ is the transposition operator) be the set of image coefficients in a single block in the watermark domain. The watermark consists of a randomly generated sequence of numbers, $\mathbf{w} = [w_1, w_2, \cdots, w_N]^T$ with a given statistical distribution. The spread spectrum watermark is embedded into the coefficients $\mathbf{x}^w$ to produce the marked coefficients $\mathbf{y}^w = [y_1^w, y_2^w, \cdots, y_N^w]^T$ as follows:

$$y_i^w = x_i^w + w_i \tag{9}$$

for $i = 1, 2, \ldots, N$, where y_i^w is the ith watermarked coefficient, and the energy of w_i is small enough to preserve the perceptual fidelity of the image. In the case of blind watermark detection, the watermark $\mathbf{w}$ is detected within the signal through correlation of $\mathbf{w}$ with the compressed and marked watermark domain coefficients of $\hat{\mathbf{y}}$. It is well known that the associated watermark channel has two sources of noise: 1) the interference from the original host image [denoted by x_i^w in (9)] and 2) the attack disturbance from the compression process [3], [4], as described in the following sections.

A. Quantization Effects on Watermarks

Eggers and Girod [14] have analyzed the quantization effects on additive watermarking schemes. A key factor for their analysis is the computation of statistical dependencies between the quantized watermarked signal and the watermark itself, which is derived by extending the theory of dithered quantizers. Their analysis on the quantization effects on additive watermarking provides a basic tool for our further investigation of spread spectrum watermarking in the presence of compression.

A model of a quantizer applied on the sum of two independent signals is shown in Fig. 2. The scalar quantization is precisely described as follows:

$$q = [u+v]_\Delta = \text{round}\left(\frac{u+v}{\Delta}\right)\Delta = u + v + e \tag{10}$$

where u is a signal such as the watermark and v is noise such as from the host image component. The variable q is the quantized signal. The function $\text{round}(\cdot)$ denotes rounding to the nearest integer, and $[\cdot]_\Delta$ represents the quantization operation with step size Δ. The quantization error e is defined as

$$e = q - u - v. \tag{11}$$

We assume that u and v are independent and they are zero mean random variables with respective probability density functions $f_u(x)$ and $f_v(x)$. Our objective is to find the expectation of the correlation coefficient between the quantized signal q and the signal u itself. From (4), this is equivalent to finding the following statistics and signal dependency

$$E\{uq\} = E\{u^2\} + E\{eu\} \tag{12}$$

$$E\{q^2\} = E\{u^2\} + E\{v^2\} + E\{e^2\} + 2E\{eu\} + 2E\{ev\}. \tag{13}$$

In [14], Eggers and Girod extended the theory of dithered quantizers and obtain elegant expressions for calculating $E\{eu\}$, $E\{ev\}$, and $E\{e^2\}$ based the characteristic functions of random variables u and v. The computation of the above statistical dependencies is summarized in the following. For a detailed analysis, please refer to [14] or to the Appendix in [20].

$$\frac{E\{e^2\}}{\frac{\Delta^2}{12}} = 1 + 12\sum_{b=1}^{\infty}\frac{(-1)^b}{\pi^2 b^2} M_{\tilde{u}}(j2\pi b\mu) M_{\tilde{v}}(j2\pi b\nu) \tag{14}$$

$$\frac{E\{eu\}}{\sigma_u^2} = \sum_{b=1}^{\infty}\frac{(-1)^b}{\pi b\mu} Im\left\{M_{\tilde{u}}^{(1)}(j2\pi b\mu)\right\} M_{\tilde{v}}(j2\pi b\nu) \tag{15}$$

$$\frac{E\{ev\}}{\sigma_v^2} = \sum_{b=1}^{\infty}\frac{(-1)^b}{\pi b\nu} M_{\tilde{u}}(j2\pi b\mu) Im\left\{M_{\tilde{v}}^{(1)}(j2\pi b\nu)\right\} \tag{16}$$

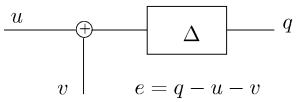

Fig. 2. Scalar quantizer with step Δ applied on the sum of two independent signals.

where σ_u and σ_v are the standard deviation of random variables u and v, respectively; $\mu = \sigma_u/\Delta$ and $\nu = \sigma_v/\Delta$ are normalized parameters; $\tilde{u} = u/\sigma_u$ and $\tilde{v} = v/\sigma_v$ are normalized random variables of u and v; $M_{\tilde{u}}(ju)$ and $M_{\tilde{v}}(jv)$ are the characteristic functions of random variables $\tilde{u}$ and $\tilde{v}$, respectively. We recall the definition of the characteristic function of a random variable y as $M_y(ju) = E\{e^{juy}\} = \int_{-\infty}^{\infty} f_y(y)e^{juy}dy$; $M_y^{(k)}(ju)$ is the kth derivative of the characteristic function, which is the integral $\int_{-\infty}^{\infty} y^k f_y(y)e^{juy}dy$.

B. Watermark Correlation of Spread Spectrum Watermarking in the Presence of Compression

In this section, we incorporate the model discussed in Section III-A into our analysis framework and derive the watermark correlation coefficients as a function of T_w and T_c.

Fig. 3 shows an alternative representation of Fig. 1 where T_w and T_c are both orthogonal transformation matrices. Spread spectrum embedding in the watermark domain T_w is equivalent to an addition in the compression domain T_c because the transformations T_w and T_c are linear. We consider vector representations for the signals where a 64 dimensional column vector is acquired from an 8×8 image block by a columnwise scanning. We let $N = 64$, $\mathbf{x} = [x_1, x_2, \cdots, x_N]^T$ be a host image block in the pixel domain, $\mathbf{x}^c = [x_1^c, x_2^c, \cdots, x_N^c]^T$ be the host image block coefficients in the compression domain, $\mathbf{w} = [w_1, w_2, \cdots, w_N]^T$ be the watermark signal in the watermark domain, and $\hat{\mathbf{y}}^c = [\hat{y}_1^c, \hat{y}_2^c, \cdots, \hat{y}_N^c]$ be the quantized watermarked signal in the compression domain. The quantized watermarked signal $\hat{\mathbf{y}}^c$ is transformed into the watermark domain for extraction. The extracted watermark $\hat{\mathbf{w}}$ is the quantized watermarked image coefficient in the watermark domain $\hat{\mathbf{y}}^w$ itself in *blind* watermarking where the original host image is not available.

From Fig. 3, we see that the watermark signal and the host image signal in the compression domain are

$$\mathbf{w}^c = T_c T_w^{-1}\mathbf{w} \tag{17}$$

$$\mathbf{x}^c = T_c\mathbf{x} \tag{18}$$

and the extracted watermark from blind extraction is

$$\hat{\mathbf{w}} = \hat{\mathbf{y}}^w = T_w T_c^{-1}\hat{\mathbf{y}}^c. \tag{19}$$

In block-based lossy compression, quantization is applied on each coefficient of the image block to a different degree based on a given quantization table denoted by $\Delta_1, \Delta_2, \cdots, \Delta_N$. Fig. 4 shows the overall coupled parallel channel model from the embedded watermark $\mathbf{w}$ to the extracted watermark $\hat{\mathbf{w}}$. The subchannels, as previously defined, correspond to the different coefficients of the 8×8 image block in the watermark domain. The coupled relationship between the different subchannels is evident in the figure by the presence of the matrix $T = T_c T_w^{-1}$

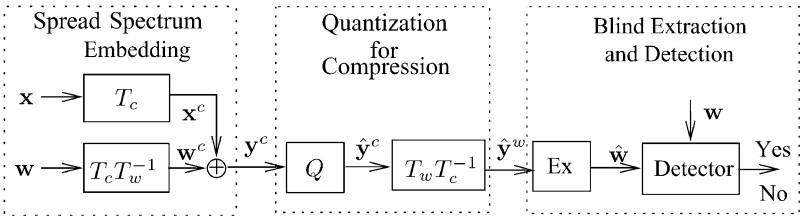

Fig. 3. Equivalent representation of the overall spread spectrum watermarking and compression processes.

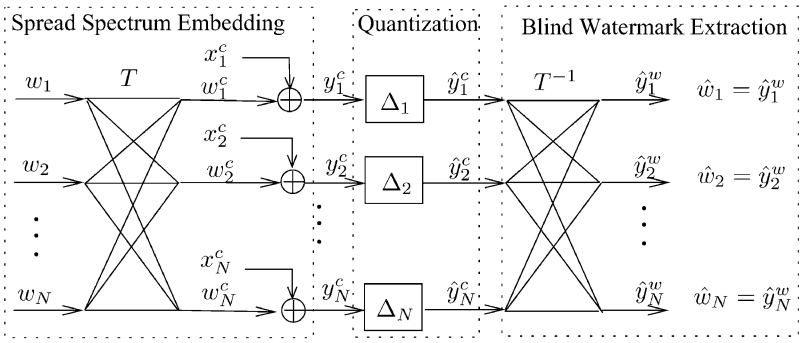

Fig. 4. Equivalent parallel additive spread spectrum watermark channel model for blind extraction.

that transforms information from the watermark domain to the compression domain where the quantization takes place after watermark embedding.

For the remainder of the paper we let $T = T_cT_w^{-1}$. Since T_w, T_c are orthogonal matrices, $T = T_cT_w^{-1}$ is also orthogonal, so that $T^{-1} = T^T$. Thus, for each channel i, from (19) the extracted watermark signal $\hat{w}_i$ is given by the following:

$$\hat{w}_i = \sum_{j=1}^{N} (T^{-1})_{ij}\hat{y}_j^c = \sum_{j=1}^{N} T_{ji}\hat{y}_j^c. \tag{20}$$

The expectation of the correlation $E\{w_i\hat{w}_i\}$ and the variance of the extracted watermark $E\{\hat{w}_i^2\}$ required in (4) can be obtained by

$$E\{w_i\hat{w}_i\} = \sum_{j=1}^{N} E\left\{T_{ji}w_i\hat{y}_j^c\right\} \tag{21}$$

$$E\left\{\hat{w}_i^2\right\} = \sum_{j=1}^{N} T_{ji}^2 E\left\{\left(\hat{y}_j^c\right)^2\right\}. \tag{22}$$

The equality of (22) holds provided that $\hat{y}_j^c, j = 1, 2, \cdots, N$ are independent of each other. In the DCT domain, the DCT coefficients $x_j^c, j = 1, 2, \cdots, N$ are almost uncorrelated, so the quantized watermarked DCT coefficients $\hat{y}_j^c$ are also almost uncorrelated. Thus, in practice, (22) is approximately true. The dependence between $w_i, i = 1, 2, \cdots, N$ for the subchannels affects the watermark correlation. Thus, we give the correlation results for two extreme cases of dependence for the subchannel inputs w_i: (Case 1) independent watermark inputs and (Case 2) fully dependent watermark inputs. Other cases result in performance between these two bounds.

1) (CASE 1) Independent Watermark Inputs: Spread Sequence: We now determine an analytic expression for correlation for the case in which w_i and w_j for $i \neq j$ are independent. This corresponds to the situation in which one long white spread spectrum watermark sequence is embedded into the image. In this situation, the watermark signals w_j, $j \neq i$ from other subchannels other than subchannel i are regarded as noise to the watermark signal w_i.

To compute the signal correlations $E\{T_{ji}w_i\hat{y}_j^c\}$ and $E\{(\hat{y}_j^c)^2\}$ in (21) and (22). We rewrite the jth quantization process in the compression domain

$$\hat{y}_j^c = \left[x_j^c + w_j^c\right]_{\Delta_j} = \left[T_{ji}w_i + x_j^c + \sum_{l=1, l\neq i}^{N} T_{jl}w_l\right]_{\Delta_j}. \tag{23}$$

Therefore, $x_j^c + \sum_{l=1,l\neq i}^{N} T_{jl}w_l$ is regarded as noise to signal $T_{ji}w_i$, so $E\{T_{ji}w_i\hat{y}_j^c\}$ and $E\{(\hat{y}_j^c)^2\}$ in (21) and (22) are obtained using (12) and (13) in Section III-A with $u = T_{ji}w_i$ and $v = x_l^c + \sum_{l=1,l\neq i}^{N} T_{jl}w_l$. $E\{w_i\hat{w}_i\}$ and $E\{\hat{w}_i^2\}$ can hence be computed.

2) (CASE 2) Fully Dependent Watermark Inputs: Watermark Repetition: Suppose $w_1, w_2, \cdots, w_N$ are fully dependent, namely for all i, $w_i = \alpha_i\tilde{w}$ where $\tilde{w} \in \mathbb{R}$ is a given realization from a specific distribution and α_i is a scaling parameter that determines the amplitude of watermark signal in channel i. This corresponds to the situation in which the watermark is repeated throughout the signal which is a common strategy to improve robustness known as "diversity" [21].

Theoretically, we can exploit the full correlation and treat the watermark components from other channels w_j, for all $j \neq i$, as equivalent to the input signal w_i. The only noise contribution

is from x_j^c. Therefore, we rewrite the jth quantization process in the compression domain

$$\begin{aligned}\hat{y}_j^c &= \left[x_j^c + w_j^c\right]_{\Delta_j} \\ &= \left[x_j^c + \sum_{l=1}^{N} T_{jl} w_l\right]_{\Delta_j} \\ &= \left[x_j^c + \left(\sum_{l=1}^{N} T_{jl}\alpha_l\right)\tilde{w}\right]_{\Delta_j}. \end{aligned} \tag{24}$$

Let $u = (\sum_{l=1}^{N} T_{jl}\alpha_l)\tilde{w}$ and $v = x_j^c$, then $E\{u\hat{y}_j^c\}$ and $E\{(\hat{y}_j^c)^2\}$ can be obtained using (12) and (13) in Section III-A. Since $E\{T_{ji}w_i\hat{y}_j^c\} = (T_{ji}\alpha_i / \sum_{l=1}^{N} T_{jl}\alpha_l)E\{u\hat{y}_j^c\}$, $E\{w_i\hat{w}_i\}$ and $E\{\hat{w}_i^2\}$ in (21) and (22) can be computed.

C. Investigative Results

To apply our analytic results for the case of JPEG compression, we let T_c correspond to the 8×8 block DCT transform. We consider the following watermark transform T_w domains: (1) pixel, i.e., the identity transform; (2) KLT; (3) DCT; (4) Hadamard transform; (5) DWT, in particular, Daubechies wavelet;[1] (6) slant transform. Given a JPEG compression quality level, the associated quantization table is fixed and known, so the expected average correlation coefficient $E\{\tilde{\rho}\}$ of each candidate transform T_w is calculated using (3), (4), (21), (22), and (23) or (24) for Cases 1 or 2, respectively.

For the simulations, a white Gaussian watermark sequence is added into the test images. For comparison, we assume that the watermark energy in all channels is equal to a constant, i.e., for all i, $E\{w_i^2\} = \sigma_{w_i}^2 = \gamma$. And in the test we choose $\gamma = 4$ for which the resulting peak-signal-to-noise ratio (PSNR) due to watermark embedding is 41.6915. The embedding distortion is small enough to guarantee imperceptibility of the watermark in our test cases. Please note that although we consider equal energy in all channels in our simulations, our models and calculations are still applicable for more sophisticated allocations of the watermark energy.

The model by Eggers and Girod in [14] shows that the probability density function (pdf) of the host data to be watermarked has a significant influence on the correlation values between the watermark and the quantized coefficient of spread spectrum watermarking. Their simulation shows that the generalized Gaussian model for DCT coefficients agrees closely with the experimental results. Thus, in order to estimate accurate theoretical results, we also adopt the generalized Gaussian distribution model for DCT coefficients of an image and the parameters of the generalized Gaussian distribution are estimated from sample data using method described in [22]. In (14)–(16), the characteristic function of the host signal v needs to be known; however, there exists no closed-form expression for the generalized Gaussian distribution. Hence, as in [14], the samples of the characteristic function of the generalized Gaussian distribution are also computed numerically in our simulations.

[1]In our experiments, we use Daubechies 4-pt wavelet filter in the first resolution and 2-pt wavelet filter in the second resolution.

(a) (b)

Fig. 5. Two test images for simulation. (a) Test image Lena. (b) Test image Mandrill.

Two real-life images are selected to assess our theoretical correlation coefficient computation. One is the classic image Lena, the other is Mandrill as shown in Fig. 5. Both cases of fully dependent and independent watermark sequences are tested.

1) Simulation Results Using Expected Average Correlation Coefficient Measure: The expected average correlation coefficient of (3) is computed to rank watermark transform domains. To evaluate how well our watermark domain ranking system based on correlation coefficient works, the average sample correlation coefficient computed by (2) and (1) is also measured from the sample images to test the relative performance of spread spectrum watermarking for different T_w in the face of JPEG compression.

Fig. 6(a) and 6(b) show the theoretical and experimental correlation coefficient results, respectively, of six different watermark transforms using the image Lena for Case 1 in which the watermark inputs in different subchannels are fully independent. Our theoretical prediction agrees closely with the experimental results. From both our theoretical prediction and the experimental results, we see that the KLT and DCT are superior to the other transforms. The slant performs better than the Hadamard and wavelet transforms, and the pixel domain has the worst performance. The ranking of these transforms is evident when the JPEG quality factor is greater than 75. However, when the quality factor becomes low, corresponding to a high compression case, the performance of these transforms is very close. The theoretical and experimental results using the image Mandrill for Case 1 are shown in Fig. 6(c) and 6(d), respectively. Similar ranking of these transforms is observed using this test image as well.

The theoretical prediction and experimental results for Case 2, in which the watermark inputs are fully dependent in the different subchannels, are shown in Fig. 7(a) and 7(b) for the test image Lena and Fig. 7(c) and 7(d) for the test image Mandrill. Our theoretical prediction again agrees closely with the experimental results. Both theoretical prediction and experimental results show that when JPEG compression occurs for a quality factor less than 92 as common in many applications, the Hadamard transform is much superior to the others. The wavelet transform is a little better than the KLT and DCT. The KLT and DCT is slightly better than the slant. An interesting thing is that the performance of the pixel domain is constant overall, so that its performance exceeds that of the wavelet, KLT, DCT, and slant transforms for very low-quality factors of compression.

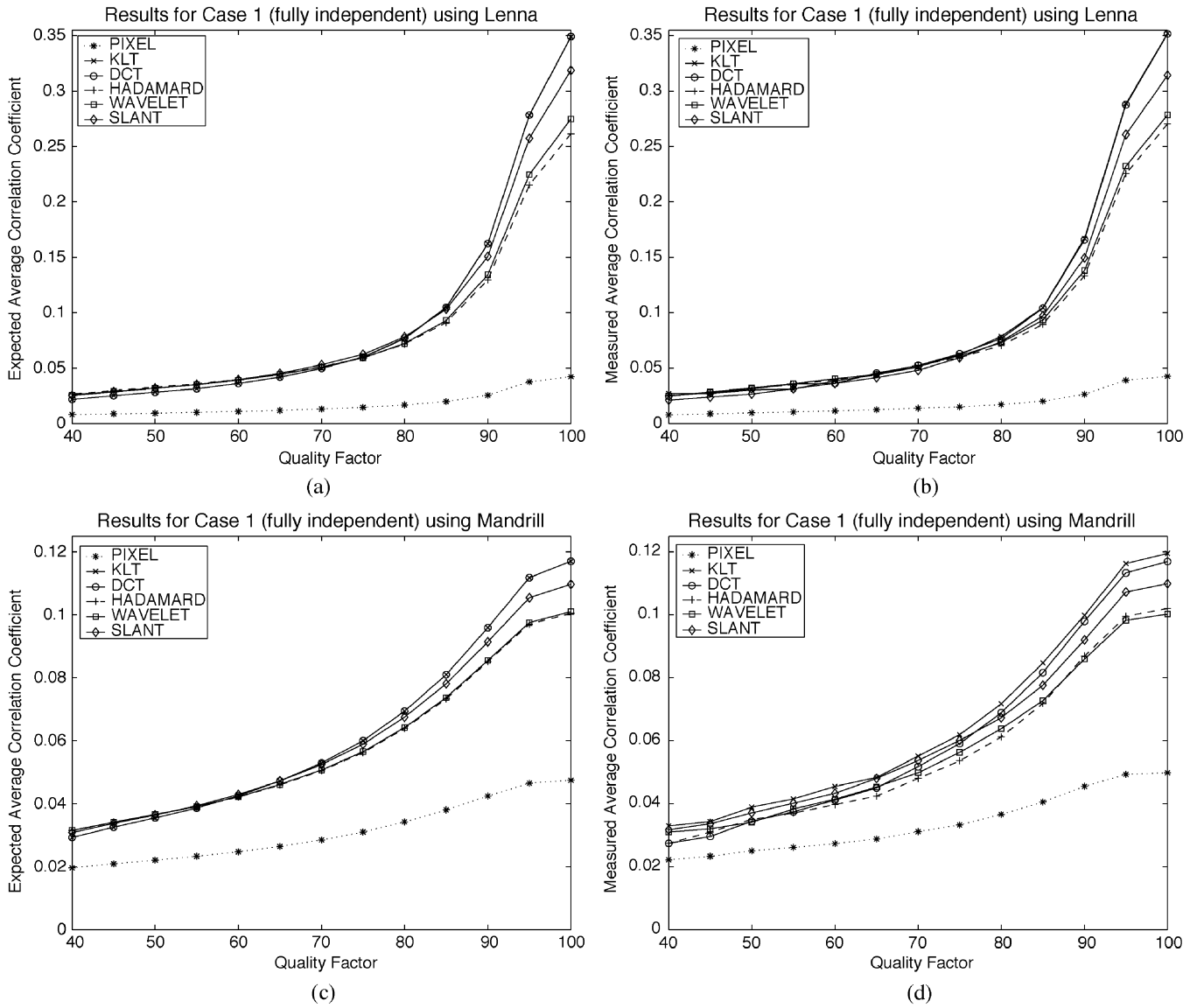

Fig. 6. Average correlation coefficient values for different spread spectrum watermarking transforms using the test images Lena and Mandrill for Case 1 (fully independent watermarks). (a) Theoretical prediction $E\{\tilde{\rho}\}$. (b) Measured average correlation coefficient $\bar{\rho}$. (c) Theoretical prediction $E\{\tilde{\rho}\}$. (d) Measured average correlation coefficient $\bar{\rho}$.

2) Simulation Results Using Watermark Detection Error Probability Measure: The second practical measure, the watermark detection error probability is also estimated to rank these transform domains. The watermark detection error probability p_e is estimated using (6), (7) and (8) which involve $Var\{w_i\hat{w}_i\}$, the variance of the correlation between the embedded watermark and the extracted watermark in subchannel i. Similar to the computation of $E\{w_i\hat{w}_i\}$ in Section III-B, the variance $Var\{w_i\hat{w}_i\}$ can be also computed based on the dithered quantizer model by Eggers and Girod in Section III-A. However some high-order statistics and signal dependencies are required for the variance computation; thus, we do not include the detailed variance analysis in the paper. For detailed analysis, please refer to [14].

In the simulations, we choose the number of image blocks for watermarking $K = 16$ for better error probability illustration. The pre-defined threshold $\mathcal{T}$ is set to be $E\{\tilde{\rho}\}/2$. When the watermark is not present in a host image, the expected average correlation coefficient is zero due to independence between watermark signal and the host image, and when the watermark is present, the expected average correlation coefficient is $E\{\tilde{\rho}\}$. Thus, it is natural to choose $E\{\tilde{\rho}\}/2$ to be a threshold of detecting whether the watermark is present or not in a host image. In our simulations, the choice of the threshold only affects the values of error probability. It does not change the rankings of these transforms.

Again, to evaluate our theoretical watermark detection error probability, the expectation and variance of the correlation coefficient in subchannels are measured from the real test images. The watermark detection error rate is then estimated from the sample expectation and variance. The theoretical detection error probability and the estimated detection error rate from the real sample image for Case 1 (fully independent watermarks) are shown in Fig. 8(a) and 8(b) for the test image Lena and Fig. 8(c) and 8(d) for Mandrill. We see that KLT and DCT have smallest detection error probability. The slant is better than Hadamard and wavelet transform, and the pixel domain is the worst again. The observation is consistent with the conclusion from the sim-

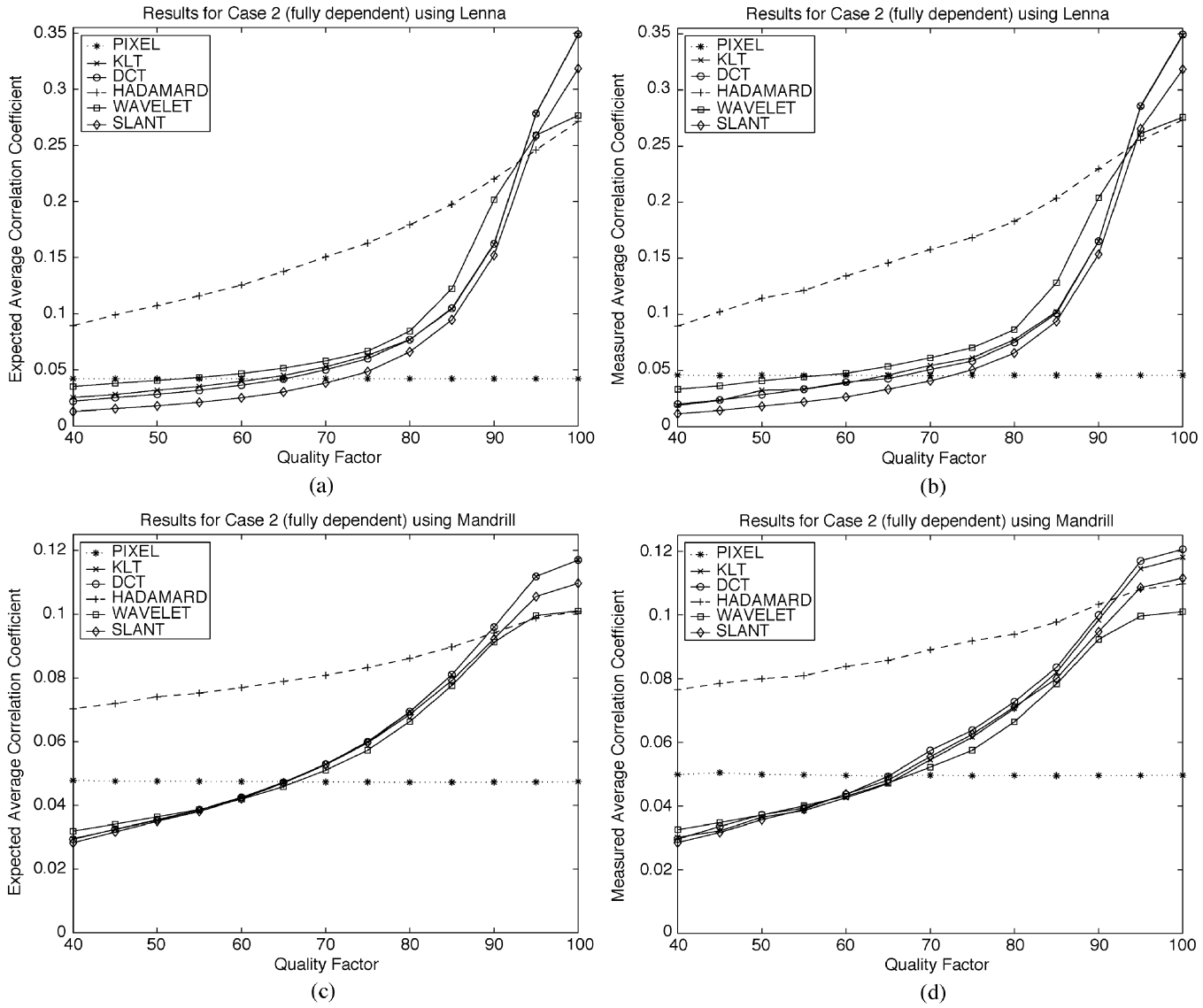

Fig. 7. Average correlation coefficient values for different spread spectrum watermarking transforms using the test images Lena and Mandrill Case 2 (fully dependent watermarks). (a) Theoretical prediction $E\{\bar{\rho}\}$. (b) Measured average correlation coefficient $\bar{\rho}$. (c) Theoretical prediction $E\{\bar{\rho}\}$. (d) Measured average correlation coefficient $\bar{\rho}$.

ulation results using the expected average correlation coefficient measure.

The theoretical prediction and experimental detection error probability results for Case 2 are shown in Fig. 9(a) and 9(b) using the test image Lena and in Fig. 9(c) and 9(d) using Mandrill, respectively. We see from both theoretical prediction and experimental results that when JPEG compression occurs for quality factors less than 92, the Hadamard transform has the smallest error probability, and is much superior to the others. The wavelet, KLT, DCT, and slant are close in behavior. Again the performance of the pixel domain stays constant, and is inferior to the wavelet, KLT, DCT, and slant transforms in high-quality factors but is superior in low-quality factors less than 60.

From these simulations, we see that our watermark detection error probability measure is consistent to the expected average correlation coefficient measure. Our theoretical predication also agrees closely with the simulation results. This reflects the accuracy of the dithered quantization model by Eggers and Girod and our satisfactory computation of a parallel array of quantizers with coupled watermark inputs. Based on the consistency of these results we believe that our measures and methodology to rank the performance of different watermarking transforms T_w is sound. In the next section, we consider the case of quantization-based watermarking and similarly deduce the ranking of different watermarking transforms in the face of JPEG compression.

IV. Quantization-Based Watermarking

In our second class of approaches, the watermark, often a binary sequence, is embedded by substituting a host signal component with a quantized value. This class of schemes is characteristic for being free of host signal interference [10], [12], [18], [23]. The purely quantize-replace embedding strategy is generally not very robust, thus, many more effective variations of quantization-based watermarking have been proposed. Among

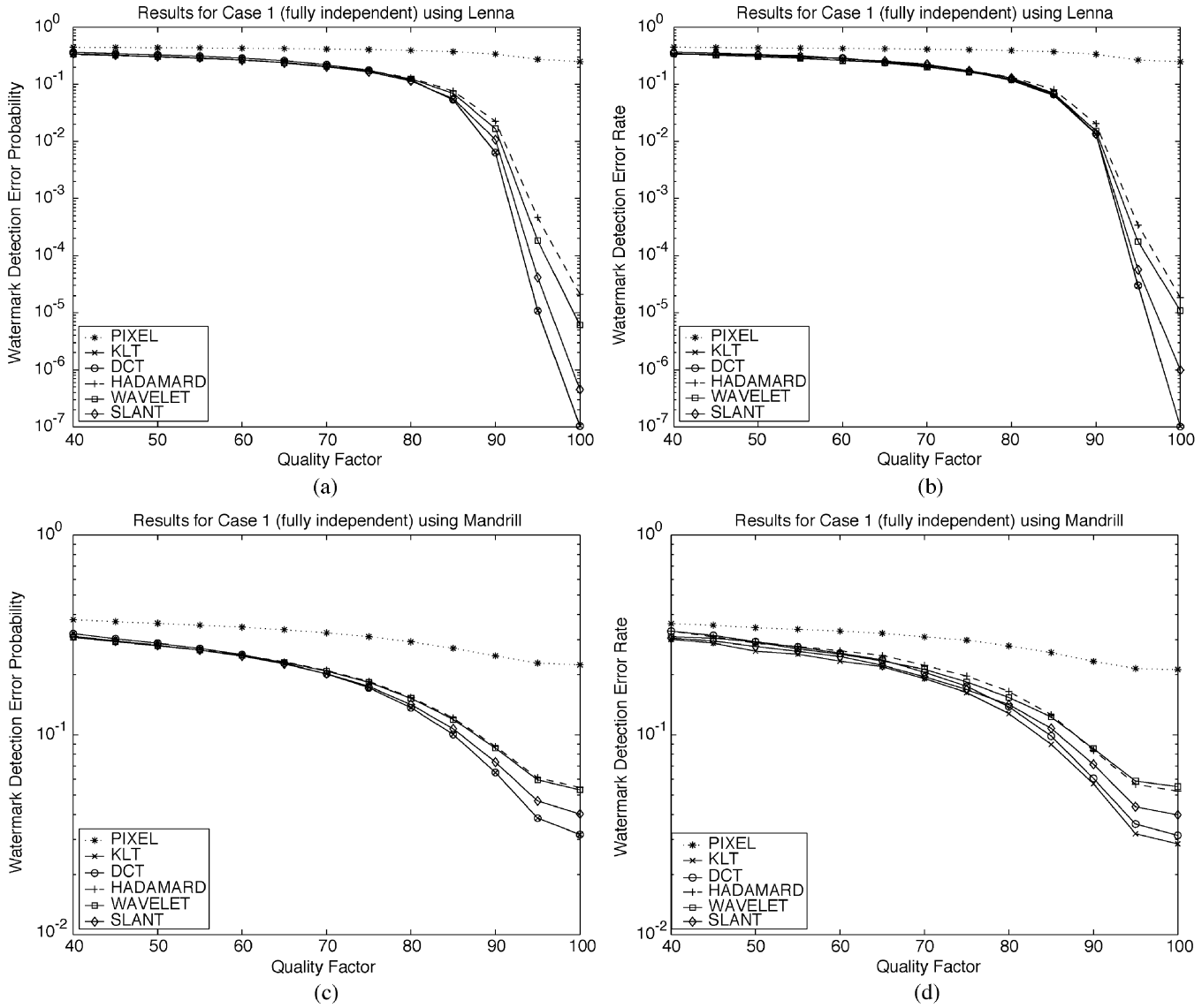

Fig. 8. Watermark detection error probability values for different spread spectrum watermarking transforms using the test images Lena and Mandrill for Case 1 (fully independent watermarks). (a) Theoretical error probability prediction. (b) Error rate estimated from test image. (c) Theoretical error probability prediction. (d) Error rate estimated from test image.

them, Eggers and Girod [19] proposed a suboptimal, but practical technique, called the Scalar Costa scheme (SCS), based on Costa's idea of achieving the channel capacity of communications with side information available to the encoder [24]. Chen and Wornell [18], [23] proposed new classes of embedding methods called quantization index modulation (QIM) and distortion-compensated QIM (DC-QIM). DC-QIM scheme is similar to the SCS, but is formulated in a different way.

We focus on the following basic method in order to evaluate the advantages that a quantization-based embedding strategy provides. The quantization-based embedding strategy we are going to evaluate is essentially a binary SCS described by Eggers and Girod or a distortion-compensated dithered modulation described by Chen and Wornell.

Let $\mathbf{x}^w = [x_1^w, x_2^w, \cdots, x_N^w]^T$ be the set of image coefficients in a single block in the watermark domain. The watermark for quantization-based watermarking consists of a randomly generated binary sequence, $\mathbf{w} = [w_1, w_2, \cdots, w_N]^T$. First, we define a dithered quantizer as follows:

$$Q_{\Delta^w}(x, w) = [x - d(w)]_{\Delta^w} + d(w) \tag{25}$$

where Δ^w is a positive real number called the quantization parameter for watermarking, $[\cdot]_{\Delta^w} = \text{round}(\cdot/\Delta^w)\Delta^w$ denotes the standard quantization operation with step size Δ^w, $d(w)$ is the dither value corresponding the watermark bit w and we choose a symmetric dither value pair $d(0) = \Delta^w/4$ and $d(1) = -\Delta^w/4$. The following assignment rule is used to embed the watermark bit w_i into the host image coefficient x_i^w to produce the watermarked coefficient y_i^w, all in the watermark domain:

$$y_i^w = Q_{\Delta^w}(x_i^w, w_i) + (1 - \alpha)e_{\Delta^w}(x_i^w, w_i) \tag{26}$$

where

$$e_{\Delta^w}(x_i^w, w_i) = x_i^w - Q_{\Delta^w}(x_i^w, w_i) \tag{27}$$

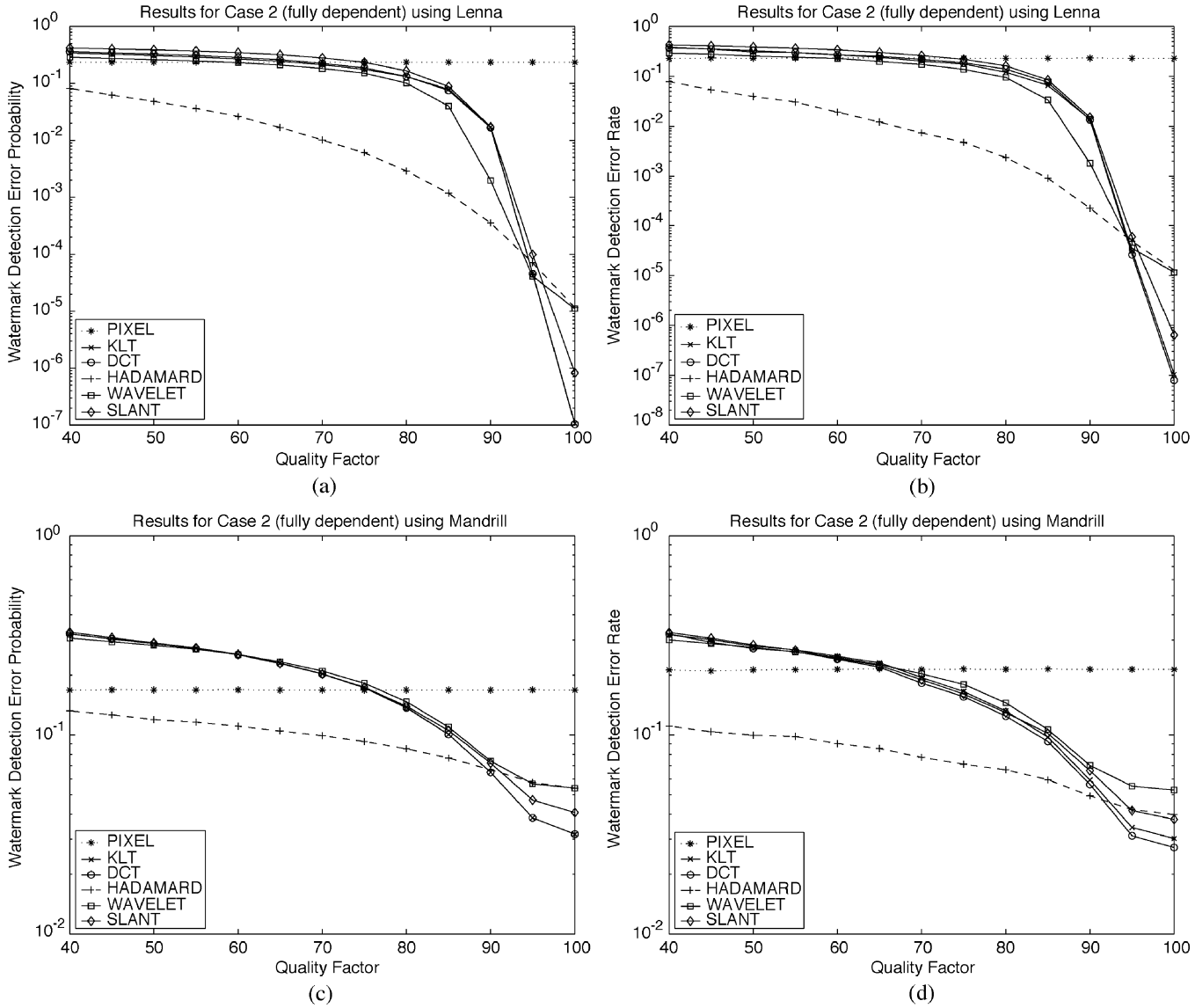

Fig. 9. Watermark detection error probability values for different spread spectrum watermarking transforms using the test images Lena and Mandrill for Case 2 (fully dependent watermarks). (a) Theoretical error probability prediction. (b) Error rate estimated from test image. (c) Theoretical error probability prediction. (d) Error rate estimated from test image.

is the quantization error due to watermark embedding. In the watermark embedding rule of (26), a fraction $1-\alpha$ of quantization error is added back to the quantization value in order to compensate for embedding distortion. The parameter α is a scalar factor $0 < \alpha \leq 1$ which determines the tradeoff between embedding distortion and robustness; and in most cases $\alpha > 0.5$.

The watermark bit is extracted blindly by the following function:

$$\hat{w}_i = \mathrm{mod}\left(\mathrm{round}\left(\frac{\hat{y}_i^w - d(0)}{\frac{\Delta^w}{2}}\right), 2\right) \tag{28}$$

where $\hat{y}_i^w$ is the "corrupted" watermarked image coefficient, $\mathrm{round}(\cdot)$ denotes integer rounding, and $\mathrm{mod}(\cdot, 2)$ represents the modulo 2 operation. When $\alpha > 0.5$, the embedded watermark bit w_i can be extracted correctly from the watermarked image coefficient y_i^w. Thus, watermark extraction for quantization-based watermarking is perfect in contrast to blind spread spectrum watermarking in which the host signal provides a source of distortion even when no attack is applied to the watermarked signal. In the next section, we model the effects of compression and apply the results to our correlation analysis.

A. *Quantization Noise*

The effect of compression is analogous to watermarking and is also achieved by quantizing the signal coefficients, but in the compression domain. Specifically, the marked signal is transformed with T_c and the individual coefficients are each passed through the following uniform scalar quantizer with step size Δ^c; the step size in general varies for each coefficient:

$$\hat{y}^c = [y^c]_{\Delta^c} = \mathrm{round}\left(\frac{y^c}{\Delta^c}\right)\Delta^c \tag{29}$$

where y^c is a watermarked image coefficient in the T_c domain, $\hat{y}^c$ is the quantized result, and $\mathrm{round}(\cdot)$ denotes rounding to the nearest integer.

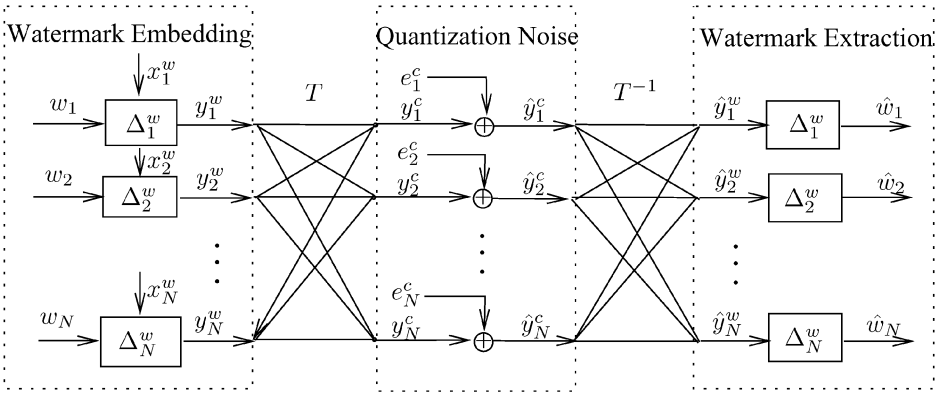

Fig. 10. Quantization-based watermarking and compression processes.

The general quantization process can be treated as an additive model for purposes of tractable correlation analysis. We define the notion of "quantization error" denoted by e^c and employ the following additive model:

$$\hat{y}^c = y^c + e^c \tag{30}$$

where the quantization error $e^c = \hat{y}^c - y^c = [y^c]_{\Delta c} - y^c$ is defined as the difference between the quantized and original signal coefficient. Suppose the probability density function (pdf) of y^c is $f_{y^c}(y)$, the pdf of the quantization error e is given by [14]

$$f_e(v) = \text{rect}\left(\frac{v}{\Delta^c}\right) \sum_{k=-\infty}^{\infty} f_{y^c}(k\Delta^c - v) \tag{31}$$

where $\text{rect}(v) = \begin{cases} 1, & \text{if } |v| \le 0.5 \\ 0, & \text{if } |v| > 0.5 \end{cases}$. The quantization noise of (31) characterizes our watermark communication channel for which we determine the watermark correlation in the next section.

B. Watermark Correlation of Quantization-Based Watermarking in the Presence of Compression

Using the same methodology as Section III-B, we begin by employing a model for the effective watermark channel characterized by the 8×8 block-based lossy compression process in the T_c domain. Once again, we assume that watermarking also occurs in a synchronized 8×8 block-based T_w domain, deal with a 64 dimensional column vector generated by columnwise scanning of 8×8 block in our analysis, and make use of the notion of subchannels for each coefficient as defined in Section II-B. In quantization-based watermarking, a binary watermark sequence is embedded. Thus, unlike spread spectrum watermarking, we model quantization-based embedding and extraction as a binary symmetric channel (BSC).

Fig. 10 presents our equivalent watermark channel model for quantization-based watermarking in the presence of lossy compression where we let $N = 8^2 = 64$. This model has two distinct differences from that of Section III-B for spread spectrum watermarking. The first is that there is no host signal interference. The second is the additive noise model for quantization due to compression in the compression domain. The vector $\mathbf{x}^w = [x_1^w, x_2^w, \cdots, x_N^w]^T$ is a host image T_w coefficient block, and $\mathbf{w} = [w_1, w_2, \cdots, w_N]^T$ is the binary watermark sequence. Watermark embedding occurs in the T_w domain; each watermark bit w_i is embedded in the corresponding image coefficient x_i^w using the embedding algorithm of (26) with step size Δ_i^w that yields the resulting watermarked coefficient y_i^w.

A transformation must be made to the T_c domain (shown in Fig. 10 through the coupling of the subchannels between the three different stages) to employ our additive quantization noise model. The extracted watermark bit $\hat{w}_i$ is obtained from the "corrupted" watermarked image coefficient $\hat{y}_i^w$ in watermark domain using the extraction process of (28) with the same parameter Δ_i^w.

Let $\mathbf{y}^c = [y_1^c, y_2^c, \ldots, y_N^c]^T$ be the coefficients of the watermarked image in the compression domain. We see that $\mathbf{y}^c = T_c T_w^{-1} \mathbf{y}^w$. If we let $T = T_c T_w^{-1}$. Then, we have

$$\mathbf{y}^c = T\mathbf{y}^w. \tag{32}$$

Let the quantization noise vector in a coefficient block be $\mathbf{e}^c = [e_1^c, e_2^c, \cdots, e_N^c]^T$, and the resulting quantized signal coefficient vector be $\hat{\mathbf{y}}^c = [\hat{y}_1^c, \hat{y}_2^c, \cdots, \hat{y}_N^c]^T$, then

$$\hat{\mathbf{y}}^c = \mathbf{y}^c + \mathbf{e}^c = T\mathbf{y}^w + \mathbf{e}^c. \tag{33}$$

By applying T^{-1} to transform $\hat{\mathbf{y}}^c$ back from the compression domain to watermark domain, the "corrupted" watermarked coefficients $\hat{\mathbf{y}}^w = [\hat{y}_1^w, \hat{y}_2^w, \cdots, \hat{y}_N^w]^T$ are obtained as follows:

$$\hat{\mathbf{y}}^w = T^{-1}\hat{\mathbf{y}}^c = \mathbf{y}^w + T^{-1}\mathbf{e}^c. \tag{34}$$

That is, the total distortion on watermarked signal $\mathbf{y}^w$ is a linear combination of quantization noises due to compression in the DCT domain

$$\hat{y}_i^w = y_i^w + \sum_{j=1}^{N} (T^{-1})_{ij} e_j^c = y_i^w + \sum_{j=1}^{N} T_{ji} e_j^c. \tag{35}$$

Applying the extraction algorithm of (28) on $\hat{\mathbf{y}}^w$, the watermark $\hat{\mathbf{w}} = [\hat{w}_1, \hat{w}_2, \cdots, \hat{w}_N]^T$ is estimated. The standard quantization operation guarantees that $[y_i^w - d(w_i)]_{\Delta_i^w} = k\Delta_i^w$, where k is an integer, and Δ_i^w is the quantization parameter for watermarking in channel i. Therefore, we deduce the relation

in (36), found at the bottom of the page, between the original watermark w_i and the extracted watermark $\hat{w}_i$ for subchannel i. The crossover bit error probability in channel i is given by (37) and (38), also shown at bottom of page. Since the quantization error pdf is symmetric and centered at the origin, and the dither values $d(0) = \Delta_i^w/4$ and $d(1) = -\Delta_i^w/4$, the above two bit-error probabilities are equal and denoted by a single crossover bit error probability p_{ei} as follows:

$$p_{ei} = P\left\{\mathrm{mod}\left(\mathrm{round}\left(\frac{(1-\alpha)e_{\Delta_i^w}(x_i^w,0)+\sum_{j=1}^{N}T_{ji}e_j^c}{\frac{\Delta_i^w}{2}}\right),2\right)=1\right\}. \tag{39}$$

From the above expression of bit-error probability, we see that two types of noises that cause watermark extraction error: one is $e_{\Delta_i^w}(x_i^w,0)$, the self noise due to embedding quantization; the other noise $\sum_{j=1}^{N}T_{ji}e_j^c$ is due to compression quantization in DCT domain.

Due to the discrete nature of the information to be communicated a discrete communication channel model is appropriate. Transmission of one watermark bit through the ith discrete subchannel can be modeled as a BSC [25] with crossover error probability p_{ei}. We consider each bit of the embedded watermark w_i for $i = 1, 2, \ldots, N$, to pass through a BSC with bit error probability p_{ei} to produce the corresponding extracted watermark bit $\hat{w}_i$. The entire process can be modeled as a system of BSCs, as shown in Fig. 11.

We consider the case that the binary watermark sequence w_i, $i = 1, 2, \cdots, N$ in different subchannels are independent. Because the DCT coefficients of a host image are almost uncorrelated, the corresponding quantization noise elements, $e_1^c, e_2^c, \cdots, e_N^c$ can be assumed to be independent of each other also. Although it is not strictly correct because of the correlation of the compression quantization noise $e_1^c, e_2^c, \cdots, e_N^c$ with the

$$\begin{aligned}
\hat{w}_i &= \mathrm{mod}\left(\mathrm{round}\left(\frac{\hat{y}_i^w - d(0)}{\frac{\Delta_i^w}{2}}\right),2\right)\\
&= \mathrm{mod}\left(\mathrm{round}\left(\frac{y_i^w + \sum_{j=1}^{N}T_{ji}e_j^c - d(0)}{\frac{\Delta_i^w}{2}}\right),2\right)\\
&= \mathrm{mod}\left(\mathrm{round}\left(\frac{[x_i^w - d(w_i)]_{\Delta_i^w} + d(w_i) + (1-\alpha)e_{\Delta_i^w}(x_i^w, w_i) + \sum_{j=1}^{N}T_{ji}e_j^c - d(0)}{\frac{\Delta_i^w}{2}}\right),2\right)\\
&= \mathrm{mod}\left(2k + \mathrm{round}\left(\frac{d(w_i) - d(0) + (1-\alpha)e_{\Delta_i^w}(x_i^w, w_i) + \sum_{j=1}^{N}T_{ji}e_j^c}{\frac{\Delta_i^w}{2}}\right),2\right)\\
&= \mathrm{mod}\left(\mathrm{round}\left(\frac{d(w_i) - d(0) + (1-\alpha)e_{\Delta_i^w}(x_i^w, w_i) + \sum_{j=1}^{N}T_{ji}e_j^c}{\frac{\Delta_i^w}{2}}\right),2\right)
\end{aligned} \tag{36}$$

$$P\{\hat{w}_i = 1 | w_i = 0\} = P\left\{\mathrm{mod}\left(\mathrm{round}\left(\frac{(1-\alpha)e_{\Delta_i^w}(x_i^w,0)+\sum_{j=1}^{N}T_{ji}e_j^c}{\frac{\Delta_i^w}{2}}\right),2\right)=1\right\} \tag{37}$$

$$P\{\hat{w}_i = 0 | w_i = 1\} = P\left\{\mathrm{mod}\left(\mathrm{round}\left(\frac{d(1) - d(0) + (1-\alpha)e_{\Delta_i^w}(x_i^w,1)+\sum_{j=1}^{N}T_{ji}e_j^c}{\frac{\Delta_i^w}{2}}\right),2\right)=0\right\} \tag{38}$$

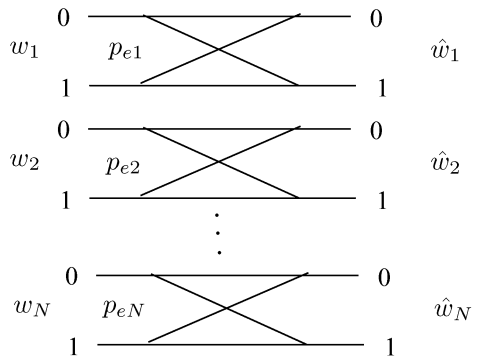

Fig. 11. Parallel BSCs used to model quantization-based embedding in the presence of compression.

self noise $e_{\Delta_i^w}(x_i^w, 0)$, we assume that these types of noises are also independent. This is a good approximation because generally the embedding quantization is much finer than the compression quantization and in most cases, the parameter $\alpha > 0.5$, so the scaling factor $1 - \alpha$ on the embedding noise $e_{\Delta_i^w}(x_i^w, 0)$ is small.

The pdf of the quantization noise, $f_{e_i^c}(v)$, is computed according to (31) with parameter $\Delta^c = \Delta_i^c$ representing the quantization step. The pdf of the self noise $f_{e_{\Delta_i^w}(x_i^w,0)}(v)$ is also computed likewise. Hence, the crossover bit-error probability in channel i, $1 \le i \le N$, is given by

$$p_{ei} = E_{e_i^w, e_1^c, e_2^c, \cdots, e_N^c} \left\{ \text{mod}\left(\text{round}\left(\frac{(1-\alpha)e_i^w + \sum_{j=1}^{N} T_{ji} e_j^c}{\frac{\Delta_i^w}{2}} \right), 2 \right) \right\} \quad (40)$$

where e_i^w denotes the self noise $e_{\Delta_i^w}(x_i^w, 0)$. $E_{e_i^w, e_1^c, e_2^c, \cdots, e_N^c}\{\cdot\}$ is the expectation operator with respect to random variables $e_i^w, e_1^c, e_2^c, \cdots, e_N^c$.

Since the binary distribution takes values on $\{0, 1\}$, which is not a zero-mean distribution, it is easy to compute the expectation and variance of correlation coefficient between the embedded watermark sequence and the extracted watermark sequence in subchannel i by mapping binary distribution to antipolar distribution on $\{-1, 1\}$. Thus, the expectation and variance of correlation coefficient in (4) and (6) is given by

$$E\{\rho_i\} = 1 - 2p_{ei} \quad (41)$$

$$Var\{\rho_i\} = \frac{4p_{ei}(1 - p_{ei})}{K} \quad (42)$$

where K is the number of image blocks for watermarking.

C. Simulation Results

To verify our theoretical observations, we rank the same transforms discussed in Section III-C using theoretical and experimental average correlation coefficient measure and watermark detection error probability measure. Results for both test images Lena and Mandrill are presented. For consistency, we assume that the quantization parameters Δ_i^w of the embedding process in different channels are all equal to a constant Δ^w, i.e. for all i, $\Delta_i^w = \Delta^w$. We set the parameter $\alpha = 0.9$, and experimentally choose $\Delta^w = 7.7$. The resulting PSNR due to watermark embedding is 41.7, so the embedding distortion is small enough to guarantee imperceptibility of the watermark embedding. The same number of image blocks for watermarking K and pre-defined threshold $\mathcal{T}$ are chosen as in the spread spectrum watermarking simulations.

Again experimental results of average correlation coefficient and watermark detection error rate are also estimated by measuring the crossover bit error probability p_{ei} from the real test images. Figs. 12 and 13 show the comparison between our theoretical prediction and the simulation results for the test images Lena and Mandrill, respectively. Overall, our theoretical results nearly follow the experimental results.

Both theoretical results in Fig. 12(a) for Lena and Fig. 12(c) for Mandrill and simulation results in Fig. 12(b) for Lena and Fig. 12(d) for Mandrill demonstrate that in high-quality factors greater than 90, the DWT is better than the slant and Hadamard, and the DCT and the KLT are the worst. The pixel domain is not bad in very high-quality factors, however deteriorates to be the worst transform in low-quality factors. Thus, unlike spread spectrum watermarking, these transforms have different behaviors in quantization-based watermarking schemes. We also see that for all transforms, the expected average correlation coefficient decreases sharply as the JPEG quality factor decreases. Hence, in low-quality factor ranges, the performance curves of these transforms are so close that it is hard to tell the difference. Although the quantization-based algorithm can extract the original watermark perfectly when the watermarked image experiences no distortions in transmission, the watermark information is severely destroyed for high degrees of compression. Thus, the quantization-based method is not very robust to JPEG compression which also confirms why it often applies to fragile watermarking schemes [26]. Therefore, the performance improvement by choosing an appropriate transform is not significant as a result of the sharp deterioration of performance.

V. Hybrid Watermarking

A. Motivation

From our analysis, it is clear that spread spectrum and quantization-based watermarking schemes have different characteristics of robustness to JPEG compression. spread spectrum watermarking is more robust to higher levels of JPEG compression while quantization watermarking does not experience host signal interference which dominates for low compression ratios.

Most block-based compression algorithms involve varying degrees of quantization for different coefficients of the 8×8 block. This motivates the idea of adopting different embedding methods for different coefficients of the host signal to increase the robustness of the data embedding scheme. We propose a hybrid watermarking algorithm that exploits the best of both watermarking methods. For compatibility with JPEG, we consider 8×8 blocks for the remainder of the work and predict, by employing our analysis, the better embedding scheme for a given coefficient in the block.

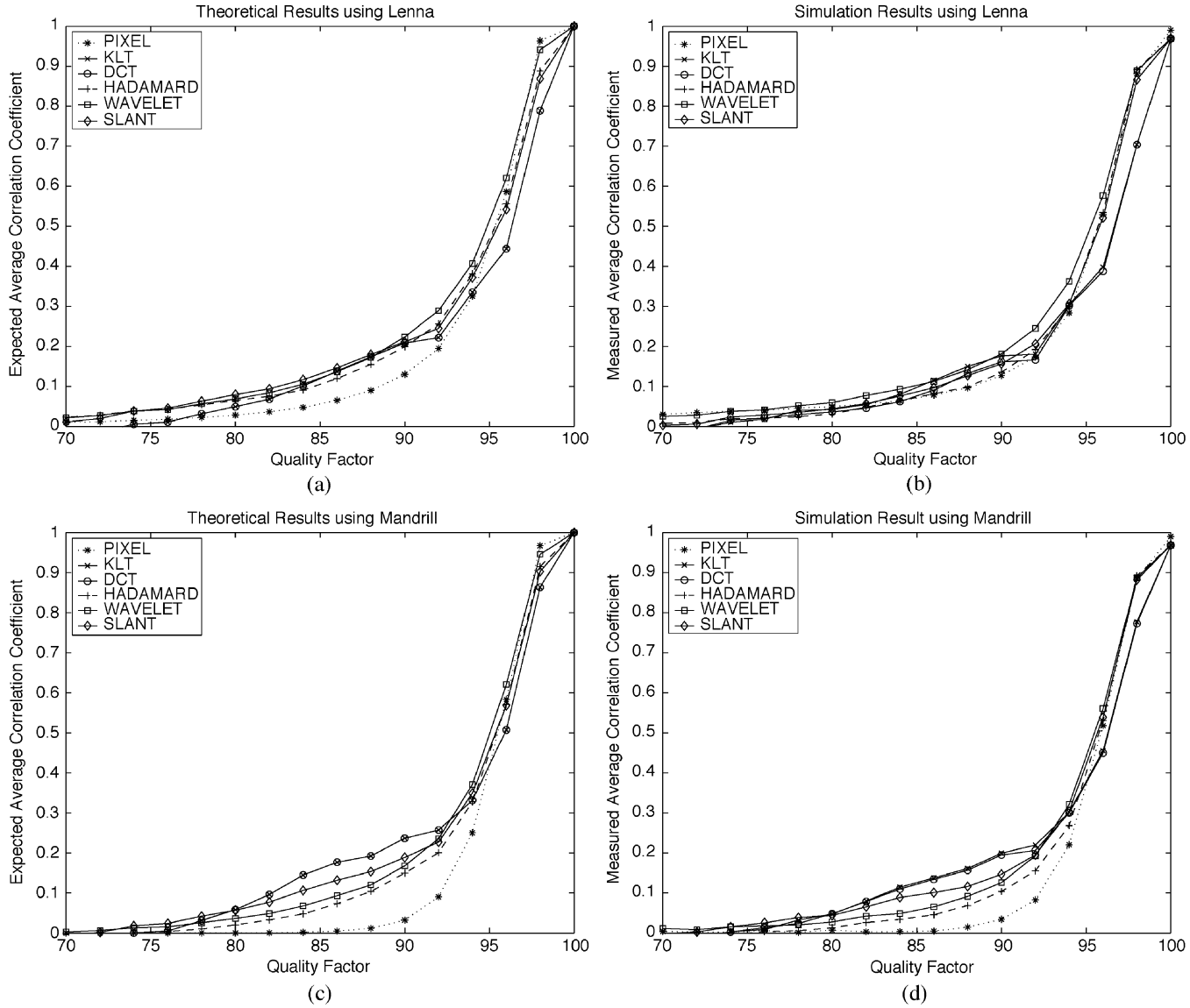

Fig. 12. Average correlation coefficient values for different quantization-based watermarking transforms using the test images Lena and Mandrill. (a) Theoretical prediction $E\{\bar{\rho}\}$. (b) Measured average correlation coefficient $\bar{\rho}$. (c) Theoretical prediction $E\{\bar{\rho}\}$. (d) Measured average correlation coefficient $\bar{\rho}$.

B. Switching Table

We introduce the notion of a *switching table* in order to assign a particular embedding method for a given coefficient. There is a one-to-one correspondence between each element in S and each coefficient band. Specifically, the table is an 8×8 matrix whose elements $S(i,j)$, $1 \le i, j \le 8$ each have a binary value $\{0, 1\}$ with the following meaning.

```
If S(i,j) = 0
  Embed the watermark in the coef-
ficient band (i, j) using the spread
spectrum method
If S(i,j) = 1
  Embed the watermark in the coeffi-
cient band (i, j) using the quantiza-
tion-based method
```

In order to compare the robustness of both embedding strategies objectively, we fix the energies of the resulting spread spectrum and quantization watermarks to be identical using the following empirical relationship:

$$\Delta^w = \frac{2\sqrt{3}\sigma_w}{\alpha} \tag{43}$$

where σ_w^2 is the variance of the Gaussian spread spectrum watermark and Δ^w is the step size for quantization watermarking. α is the parameter for quantization embedding of (26).

For straightforward performance comparison, the expectation of correlation coefficient between the original and extracted watermarks is used as an objective measure of robustness. We let ρ_{ij}^S, $1 \le i, j \le 8$ be the expected correlation coefficient of the original and extracted watermark in the coefficient band (i, j) using the spread spectrum method. The value of ρ_{ij}^S is computed by (4), (21), (22) and (23) (for Case 1) or (24) (for Case 2) in Section III-B, where $8j + i$ is the index of the subchannel in the column vector representation corresponding to coefficient band (i, j).

We let ρ_{ij}^Q, $1 \le i, j \le 8$ be the expected correlation coefficient for the quantization-based method. The value of $\rho^Q(i,j)$

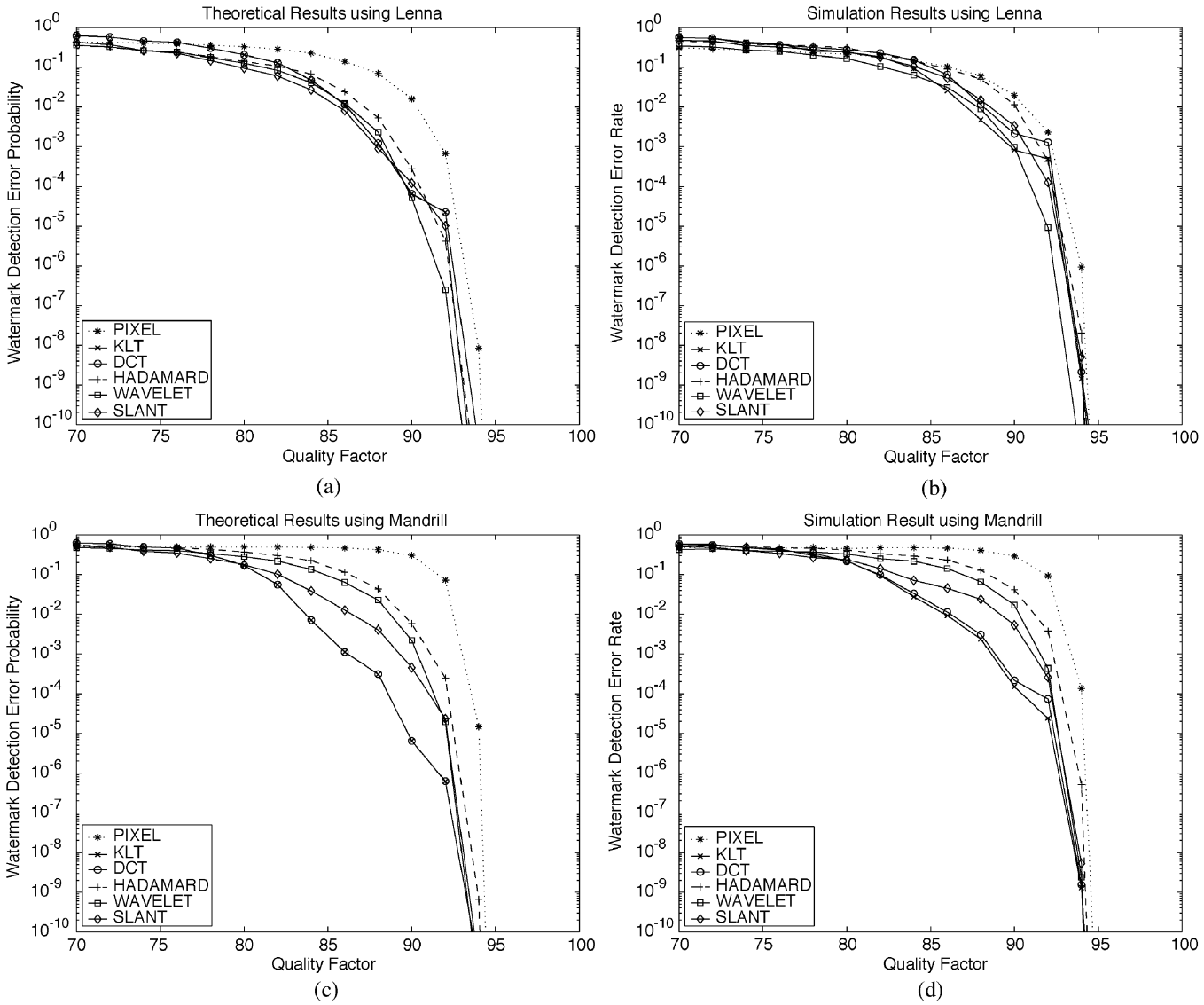

Fig. 13. Watermark detection error probability values for different quantization-based watermarking transforms using the test images Lena and Mandrill. (a) Theoretical detection error probability prediction. (b) Detection error rate estimated from the sample image. (c) Theoretical detection error probability prediction. (d) Detection error rate estimated from the sample image.

TABLE I
HYBRID WATERMARK GENERATOR ALGORITHM

If $S(i,j)=0$, then

For all $1 \le k \le K$, generate $w_{ij}(k)$ randomly with a given distribution such as Gaussian $\mathcal{N}(0,\sigma_w^2)$.

If $S(i,j)=1$, then

For all $1 \le k \le K$, generate $w_{ij}(k)$ randomly with equi-probable binary distribution.

is calculated by (41) in Section IV-B with a crossover bit error probability p_{ei} obtained from (40). Again $8j+i$ is the index of the subchannel in the column vector representation corresponding to coefficient (i, j). Using these predicted measures, the switching table is generated prior to embedding through the following comparison:

$$S(i,j)=\begin{cases}0, & \text{If } \rho_{ij}^{S} > \rho_{ij}^{Q}\\ 1, & \text{If } \rho_{ij}^{S} < \rho_{ij}^{Q}\\ 0 \text{ or } 1, & \text{If } \rho_{ij}^{S} = \rho_{ij}^{Q}\end{cases}. \tag{44}$$

C. Algorithm

Let $x_{ij}^{w}(k)$ be the image coefficient located at (i, j) in the kth block in the T_w domain, $w_{ij}(k)$ be the watermark for $1 \le i, j \le 8, 1 \le k \le K$ where K is the total number of 8×8 image blocks. Let σ_w and Δ^w be the embedding parameters satisfying (43). The watermark signal sequence $w_{ij}(k)$ is independently generated as shown in Table I to suit the characteristics of the particular embedding strategy for each 8×8 image block coefficient. Spread spectrum watermark generation corresponding to Case 1 is employed.

TABLE II
HYBRID WATERMARK EMBEDDING ALGORITHM

1) A linear orthogonal transformation T_w is applied to each 8×8 image block of the host image to produce $x_{ij}^w(k)$, where $(i,j), 1 \leq i,j \leq 8$ denotes the position of coefficient in the kth 8×8 block.
2) For each block k, and for each $(i,j), 1 \leq i,j \leq 8$,
   a) If $S(i,j) = 0$, then embed $w_{ij}(k)$ in $x_{ij}^w(k)$ using the spread spectrum approach.

$$y_{ij}^w(k) := x_{ij}^w(k) + w_{ij}(k) \tag{45}$$

   b) If $S(i,j) = 1$, then embed $w_{ij}(k)$ in $x_{ij}^w(k)$ using the quantization based approach.

$$y_{ij}^w(k) := Q_{\Delta^w}(x_{ij}^w(k), w_{ij}(k)) + (1-\alpha)(x_{ij}^w(k) - Q_{\Delta^w}(x_{ij}^w(k), w_{ij}(k))) \tag{46}$$

   where the dithered quantizer function $Q_{\Delta^w}(x,w)$ is defined in Equation (25) and α is given.
3) The corresponding inverse transformation T_w^{-1} is applied to $y_{ij}^w(k)$ to form the watermarked image.

TABLE III
HYBRID WATERMARK EXTRACTION AND DETECTION ALGORITHM

1) Do block transform on the watermarked image to yield the watermarked image coefficients $\hat{y}_{ij}^w(k)$ in watermark domain.
2) Extraction of the watermark from the watermarked image coefficients $\hat{y}_{ij}^w(k)$ occurs as follows.
   a) If $S(i,j) = 0$, then extract the watermark information with the spread spectrum extraction algorithm. The extracted watermark is the watermarked image coefficient itself in *blind* watermarking where the original image is not available.

$$\hat{w}_{ij}(k) = \hat{y}_{ij}^w(k) \tag{47}$$

   b) If $S(i,j) = 1$, then extract the watermark bit with the following quantization based extraction algorithm

$$\hat{w}_{ij}(k) = \mathrm{mod}(\mathrm{round}(\frac{\hat{y}_{ij}^w(k) - d(0)}{\Delta^w/2}), 2) \tag{48}$$

   where $d(0) = \frac{\Delta^w}{4}$.
3) The individual correlation coefficient of each channel is calculated in the corresponding standard way as follows.
   a) If $S(i,j) = 0$,

$$\rho_{ij} = \frac{\frac{1}{K}\sum_{k=1}^{K} w_{ij}(k)\hat{w}_{ij}(k)}{\sigma_w \sqrt{\frac{1}{K}\sum_{k=1}^{K} \hat{w}_{ij}^2(k)}} \tag{49}$$

   b) If $S(i,j) = 1$,

$$\rho_{ij} = 1 - \frac{2}{K}\sum_{k=1}^{K} w_{ij}(k) \oplus \hat{w}_{ij}(k) \tag{50}$$

   where $\oplus$ denotes modulo 2 addition.
4) To detect the existence of original watermark, the average correlation coefficient $\tilde{\rho}$ is calculated over all coefficient bands

$$\tilde{\rho} = \frac{1}{8 \times 8}\sum_{i=1}^{8}\sum_{j=1}^{8} \rho_{ij}. \tag{51}$$

   To assess the existence of the original watermark, that is, to give yes-or-no watermark detection decision, we compare the average correlation coefficient $\tilde{\rho}$ to a pre-defined threshold $\mathcal{T}$,
   a) If $\rho > \mathcal{T}$, the original watermark is considered to be present;
   b) Otherwise, the original watermark is considered not to be present.

The watermark embedding and detection algorithms are detailed in Tables II and III, respectively. It should be noted that the switching table S is generated according to the predicted behaviors of the spread spectrum and quantization-based methods against perceptual coding. The switching table can be pre-computed prior to the data embedding process, so the complexity of calculating the switching table does not influence real time implementation of watermark insertion and extraction algorithms.

In the next section, we justify our use of the models introduced in Sections III and IV by verifying the improved performance of our novel hybrid scheme in comparison to standard spread spectrum and quantization-based methods.

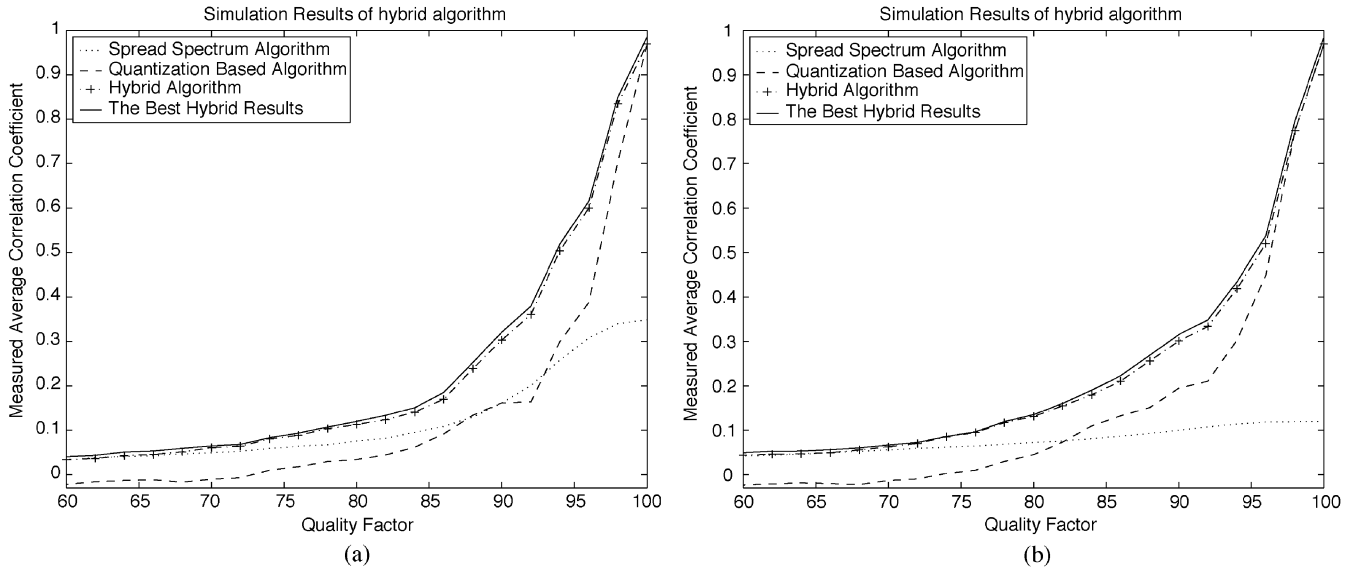

Fig. 14. The average sample correlation coefficient of (51) versus JPEG compression quality for hybrid watermarking. The dotted, dashed, dotted-dashed with "+" and solid lines represent the results for the purely quantization-based method, purely spread spectrum method, our novel hybrid method in practice, and the best hybrid results, respectively. (a) Using test image Lena. (b) Using test image Mandrill.

D. Simulations and Comparison

We present results for the two different test images used in Section III-C. We set $\sigma_w = 2$ and then $\Delta^w = 2\sqrt{3}\sigma_w/\alpha = 7.7$ from (43) to maintain imperceptibility of the watermark. The JPEG compression quality factor is assumed to be known during the watermark embedding process. The average sample correlation coefficient of (51) discussed in Table III is computed to measure the success of the watermarking scheme. The transform T_w is set to be the 8×8 DCT which provides the best performance for spread spectrum watermarking (Case 1).

Fig. 14 shows the average correlation coefficient of our hybrid algorithm compared to both the standard spread spectrum and quantization-based algorithms for JPEG quality factor ranging from 60 to 100 using the test images Lena and Mandrill. We see that for a JPEG quality factor near 100, the plot of the average correlation coefficient [given by (51)] of the hybrid algorithm is close to that of the quantization-based algorithm because under low compression conditions the host signal interference dominates to give the quantization embedding a performance advantage; the hybrid algorithm switches to the quantization-based technique in all coefficient bands. Similarly, when the quality level is less than 75, the hybrid algorithm tracks the spread spectrum method as the latter has superior performance. The solid lines in Fig. 14 represent the best results of the hybrid algorithm which corresponds to the situation in which the hybrid algorithm switches to the best embedding method in all coefficient bands. The best hybrid results are measured using the switching table obtained from sample correlation coefficients from the test image, and represent the best performance results that hybrid algorithm can achieve. We can see that our hybrid method in practice tracks the best hybrid results, which verifies that the theoretically derived switching table nearly achieves the optimal performance. The small numerical gap between our hybrid method and its best results, we believe, is because JPEG compression involves casting float numbers into integers in the pixel domain for the purpose of file storage, which inevitably introduces another form of quantization noise not modeled in our framework.

The hybrid algorithm is better than the other methods and demonstrates the advantage of tailoring the embedding method for each coefficient. This advantage comes at the cost of having to know the JPEG compression level prior to watermarking. Since watermark embedding occurs before compression in our model, it is not always practical to know the degree of coding prior to marking. We can relax this constraint by giving the embedder freedom to assume a "reasonable" compression quality factor and generate a fixed switching table. Fig. 15 shows the comparison of our hybrid algorithm using the fixed switching table with other algorithms. In Fig. 15(a), a fixed switching table derived using a quality factor 95 is applied. Optimal performance is achieved for a quality of 95, but the scenario is not as ideal for other compression ratios. However, the overall result is still better than standard spread spectrum and quantization algorithms if the JPEG quality is larger than 80. Similarly, in Figs. 15(b) and 15(c), there is a performance degradation by assuming an inaccurate quality factor, but the hybrid algorithm still achieves greatest relative performance up to ± 15 of the estimated quality factor.

We have also conducted simulations to test the effect of desynchronization of the watermark and compression transform blocks. By this we mean that the 8×8 blocks are not partitioned in the same way for the T_w and T_c domains; there is a relative shift with the block partitioning. Fig. 16 shows the simulation results of relative shifts in the block partitions along rows and columns. We find that the hybrid algorithm performance is far from optimal and is worse than the purely spread spectrum quantization-based methods in the quality factor range about 90. We believe this is because in the case of desynchronization, the relative accuracy of the spread spectrum and quantization-based method models deteriorates to produce a switching table that is inaccurate.

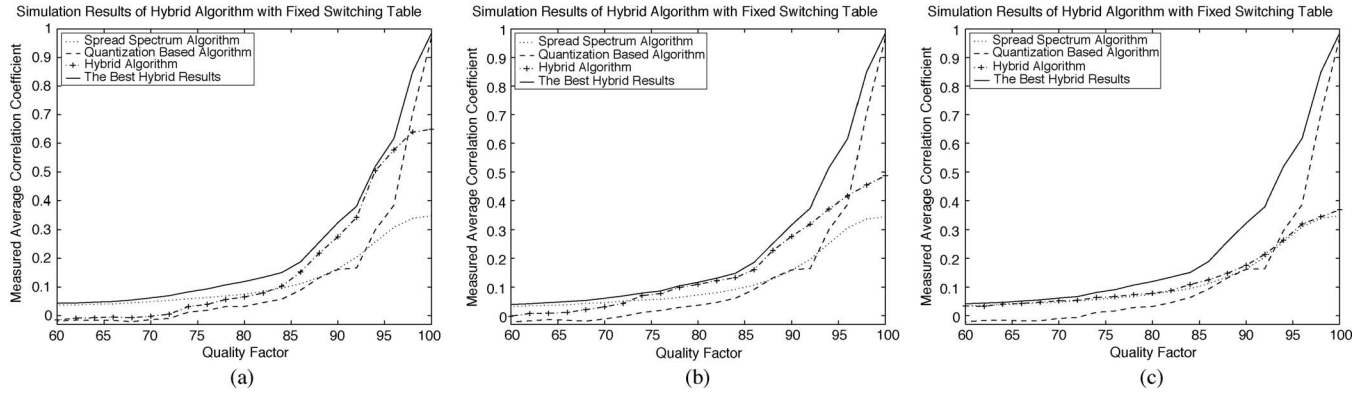

Fig. 15. Hybrid algorithm performance when switching table is fixed and derived from a given quality factor. (a) Assuming quality factor of 95. (b) Assuming quality factor of 80. (c) Assuming quality factor of 65.

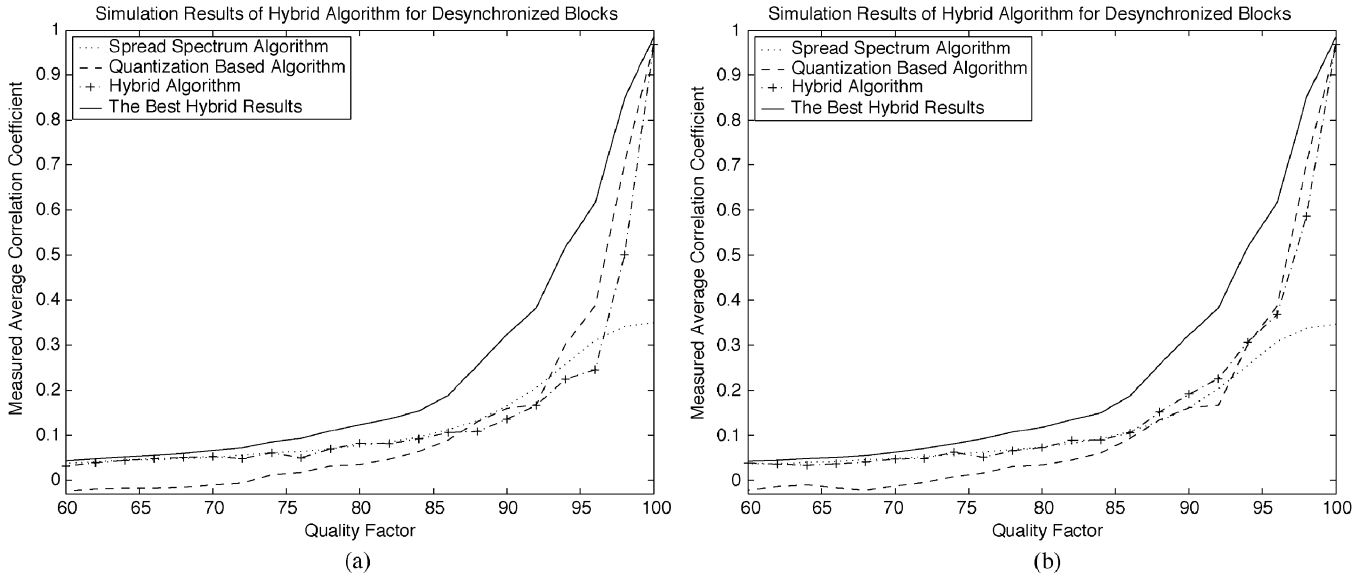

Fig. 16. Results for desynchronized 8×8 blocks for watermarking and compression using the test image Lena. (a) A relative shift of (4, 4) corresponding to the worst-case situation. (b) A relative shift of (2, 6).

E. Discussion

The process of quantization due to compression is modeled as a parallel array of quantizers. For spread spectrum watermarking where the watermark is added into the host image, the watermark quantization model by Eggers and Girod is extended for correlation coefficient analysis. For quantization-based watermarking, the quantization error due to compression as well as the self noise due to quantization embedding characterize the watermark channel. Our selection of these models traded-off ease of analysis with practical performance which was evaluated through simulations. Our use of the expected correlation coefficient measure aids in an improved hybrid algorithm design by permitting the selection of an embedding strategy from the spread spectrum and quantization-based methods for every coefficient.

In order to compare the performance of the watermarking approaches in different domains and for different embedding strategies, the watermark signal energy is held constant during embedding. Therefore, the work as presented does not take into account the different masking characteristics available for perceptually-tuned embedding in the various domains. To include this component to the work, we would need models of masking characteristics such as just noticeable difference measures for all the domains considered. Investigation of such visibility models is beyond the scope of this work. However, many watermarking algorithms used in practice employ PSNR as a measure of perceptibility and could, therefore, make use of our results.

VI. Conclusion

This paper has analyzed the performance of two typical classes of watermark embedding techniques in the presence of compression. The expected average correlation coefficient for data hiding is a function of the embedding process, the transforms used for watermarking and compression, as well as the statistics of the watermark and host signal.

Our findings show that use of spread spectrum watermarking with a repetition code, and quantization-based embedding perform well when watermarking is applied in a "complementary" domain to compression. Spread spectrum watermarking using independent watermark elements works best when the same domain is employed.

For improved robustness to JPEG compression, we propose a hybrid watermarking scheme that exploits the theoretically pre-

dicted advantages of spread spectrum and quantization-based watermarking to give superior performance.

Much of our analysis for image watermarking can be extended, in part, for video and audio embedding. However, the differences in the signal and compression models must be taken into account. Further research will attempt to extend the analysis to general multimedia watermarking.

REFERENCES

[1] R. B. Wolfgang, C. I. Podilchuk, and E. J. Delp, "The effect of matching watermark and compression transforms in compressed color images," in *Proc. IEEE Int. Conf. Image Processing*, vol. 1, Oct. 1998, pp. 440–455.

[2] D. Kundur and D. Hatzinakos, "Mismatching perceptual models for effective watermarking in the presence of compression," in *Proc. SPIE, Multimedia Systems and Application II*, vol. 3845, A. G. Tescher, Ed., Sept. 1999, pp. 29–42.

[3] M. Ramkumar and A. N. Akansu, "Theoretical capacity measures for data hiding in compressed images," in *Proc. SPIE, Voice, Video and Data Communications*, vol. 3528, Nov. 1998, pp. 482–492.

[4] M. Ramkumar, A. N. Akansu, and A. Alatan, "On the choice of transforms for data hiding in compressed video," in *IEEE ICASSP*, vol. vi, Phoenix, AZ, Mar. 1999, pp. 3049–3052.

[5] I. J. Cox, J. Killian, T. Leighton, and T. Shamoon, "Secure spread spectrum watermarking for multimedia," *IEEE Trans. Image Processing*, vol. 6, pp. 1673–1687, Dec. 1997.

[6] X. G. Xia, C. G. Boncelet, and G. R. Arce, "A multiresolution watermark for digital images," in *Proc. IEEE Int. Conf. Image Processing*, vol. 1, Nov. 1998, pp. 548–551.

[7] M. Barni, F. Bartolini, V. Cappellini, and A. Piva, "A DCT domain system for robust image watermarking," *Signal Processing*, vol. 66, pp. 357–372, 1998.

[8] F. Hartung and B. Girod, "Watermarking of uncompressed and compressed video," *Signal Processing*, vol. 66, pp. 283–801, 1998.

[9] R. B. Wolfgang, C. I. Podilchuk, and E. J. Delp, "Perceptual watermarks for digital images and video," *Proc. IEEE—Special Issue on Identification and Protection of Multimedia*, vol. 87, no. 7, pp. 1108–1126, July 1999.

[10] M. Wu, H. Yu, and A. Gelman, "Multi-level data hiding for digital image and video," in *SPIE Photonics East '99*, Boston, MA, 1999.

[11] B. Chen and G. W. Wornell, "Dither modulation: A new approach to digital watermarking and information embedding," in *Proc. SPIE: Security and Watermarking of Multimedia Contents*, vol. 3657, Jan. 1999, pp. 342–353.

[12] D. Kundur and D. Hatzinakos, "Digital watermarking using multiresolution wavelet decomposition," in *Proc. IEEE Int. Conf. Acoustics, Speech and Signal Processing*, vol. 5, Seattle, Washington, May 1998, pp. 2969–2972.

[13] J. J. Eggers and B. Girod, "Watermark detection after quantization attacks," in *Proc. 3rd Workshop on Information Hiding*, Dresden, Germany, 1999.

[14] ——, "Quantization effects on digital watermarks," *Signal Processing*, vol. 81, no. 2, pp. 239–263, Feb. 2001.

[15] M. Wu and H. Yu, "Video access control via multi-level data hiding," in *IEEE Int. Conf. Multimedia & Expo (ICME'00)*, New York, 2000.

[16] C. Fei, D. Kundur, and R. Kwong, "The choice of watermark domain in the presence of compression," in *Proc. IEEE Int. Conf. on Information Technology: Coding and Computing*, Las Vegas, NV, Apr. 2001, pp. 79–84.

[17] ——, "Transform-based hybrid data hiding for improved robustness in the presence of perceptual coding," in *Proc. SPIE: Mathematics of Data/Image Coding, Compression and Encryption IV*, vol. 4475, San Diego, CA, July 2001, pp. 203–212.

[18] B. Chen and G. W. Wornell, "Quantization index modulation: a class of provably good methods for digital watermarking and information embedding," *IEEE Trans. Inform. Theory*, vol. 47, pp. 1423–1433, May 2001.

[19] J. Eggers and B. Girod, *Informed Watermarking*. Norwell, MA: Kluwer, 2002.

[20] I. J. Cox, M. L. Miller, and J. A. Bloom, *Digital Watermarking*. New York: Morgan Kaufmann, 2002.

[21] D. Kundur and D. Hatzinakos, "Diversity and attack characterization for improved robust watermarking," *IEEE Trans. Signal Processing*, vol. 49, pp. 2383–2396, Oct. 2001.

[22] K. A. Birney and T. R. Fischer, "On the modeling of DCT and subband image data for compression," *IEEE Trans. Image Processing*, vol. 4, pp. 186–193, Feb. 1995.

[23] B. Chen, "Design and Analysis of Digital Watermarking, Information Embedding, and Data Hiding Systems," Ph.D. dissertation, MIT, Cambridge, MA, June 2000.

[24] M. Costa, "Writing on dirty paper," *IEEE Trans. Inform. Theory*, vol. 29, pp. 439–441, May 1983.

[25] D. Kundur, "Multiresolution Digital Watermarking: Algorithm and Implication for Multimedia Signals," Ph.D. dissertation, Univ. Toronto, Toronto, ON, Canada, 1999.

[26] D. Kundur and D. Hatzinakos, "Toward a telltale watermarking technique for tamper-proofing," in *Proc. IEEE Int. Conf. Image Processing*, vol. 2, Oct. 1998, pp. 409–413.

Chuhong Fei was born in Zhejiang, China. He received the B.E. and M.E. degrees from Xi'an Jiaotong University, China, in 1994 and 1997, respectively, and the M.A.Sc. degree in electrical and computer engineering in 2001, from the University of Toronto, Toronto, ON, Canada, where he is currently working toward the Ph.D. degree.

His research interests include multimedia security, data hiding, multimedia signal processing.

Deepa Kundur (M'99–SM'03) was born in Toronto, ON, Canada. She received the B.A.Sc., M.A.Sc., and Ph.D. degrees, all in electrical and computer engineering, in 1993, 1995, and 1999, respectively, from the University of Toronto, Toronto, ON, Canada.

She joined the Electrical Engineering Department, Texas A&M University, College Station, in January 2003, where she is a member of the Wireless Communications Laboratory and holds the position of Assistant Professor. From September 1999 to December 2002, she was an Assistant Professor at the Edward S. Rogers Sr. Department of Electrical and Computer Engineering, University of Toronto, where she held was Bell Canada Junior Chair-holder in Multimedia. Her research interests include multimedia and network security for digital rights management, video cryptography, data hiding and steganography, covert communications, and nonlinear and adaptive information processing algorithms.

Dr. Kundur is a Guest Editor for the PROCEEDINGS OF THE IEEE Special Issue on Enabling Technologies for Digital Rights Management. She has been on numerous technical program committees and has given tutorials at ICME 2003 and Globecom 2003 in the area of digital rights management. She received the 2002 Gordon Slemon Teaching of Design Award and the 2002 Best Electrical Engineering Professor Award (Spring) presented by the ECE Club.

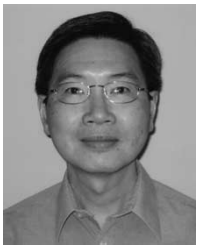

Raymond H. Kwong (M'75) was born in Hong Kong in 1949. He received the S.B., S.M., and Ph.D. degrees in electrical engineering from the Massachusetts Institute of Technology, Cambridge, in 1971, 1972, and 1975, respectively.

From 1975 to 1977, he was a visiting Assistant Professor of Electrical Engineering at McGill University, Montreal, QC, Canada, and a Research Associate at the Centre de Recherches Mathematiques, Universite de Montreal, Montreal. Since August 1977, he has been with the Edward S. Rogers Sr. Department of Electrical and Computer Engineering, University of Toronto, Toronto, ON, Canada, where he is now a Professor and Associate Chair for Undergraduate Studies. His current research interests include estimation and stochastic control, adaptive signal processing and control, fault diagnosis, discrete event systems, and hybrid systems.